

CP Violation In and Beyond The Standard Model: Two Higgs Doublet Model Type II Contributions to Flavour Observables

Matthew Rossetter

Supervised By Alexander Lenz

MPhys Theoretical Physics, Durham University

ABSTRACT: In this study, we first cover the theory of the Standard Model (SM) and then test the Two Higgs Doublet Model (2HDM) of Type II as an extension to the SM using indicative flavour observables, such as leptonic and semileptonic decays of B and D mesons, $B\bar{B}$ mixing, and the $b \rightarrow s\gamma$ radiative decay. Testing the 2HDM parameter space $(m_{H^\pm}, \tan\beta)$ to find alignment between theoretical calculations and experiment, constraints on the parameters were found for flavour phenomena to work towards a global fit. We perform this fit in both the alignment and wrong sign limits of the 2HDM. Strongly dominated by the $b \rightarrow s\gamma$ branching ratio, the mass of a charged Higgs particle would be expected to have a minimum value at 95% CL of 490 GeV in the alignment limit and 740 GeV in the wrong sign limit. The value of $\tan\beta$ is limited by $B_q \rightarrow \mu^+\mu^-$ decays, yielding maximum values at 95% CL of 20.8 in the alignment limit and 4.03 in the wrong sign, for the fixed choices of other parameters. This work was then joined with constraints from the oblique parameters S, T, U from another work, to better give judgement on the state of the 2HDM fit. The results of this combined fit are no more conclusive than flavour alone, due to additional parameter dependency in S, T, U ; the only additional constraint we definitively find here is that $m_{H^\pm} \approx m_{H^0} \approx m_{A^0}$ in both the alignment and wrong sign limits. The validity of this fit is heavily influenced by the semileptonic ratio $\mathcal{R}(D^*)$ which remains in disagreement with the 2HDM fit to 3σ ; the statistical fit of these observables points to exclusion of this model at 95% CL in the wrong sign limit, and 85% CL in the alignment limit, at 2σ error significance. This model cannot be excluded at 3σ error significance, where $\mathcal{R}(D^*)$ no longer causes disagreement in the fit.

Contents

1	Introduction	1
1.1	The Standard Model	2
1.2	Flavour Physics and CP Violation	7
1.3	The Two Higgs Doublet Model of Type II	9
2	Probing the 2HDM Type II	10
2.1	Leptonic Decays	10
2.2	Mass mixing	12
2.3	Radiative decay	13
2.4	Updating The 2HDM Constraints	14
2.5	New Observables	16
2.6	SM4 with Two Higgs Doublet Model	19
2.7	The Global Fit with Oblique Parameters	20
3	Discussion	21
3.1	Future Prospects	25
4	Conclusions	26
A	Plots of 3σ scans	30
B	Relevant Feynman Rules in the SM and 2HDM	30

1 Introduction

The Standard Model [1] is one of the most successful theories ever developed, describing the fundamental forces currently observed, excluding gravity, through a quantum field theory Lagrangian,

$$\begin{aligned}\mathcal{L} = & -\frac{1}{4}F^{\mu\nu}F_{\mu\nu} && \rightarrow \text{gauge term} \\ & +i\bar{\Psi}\not{D}\Psi && \rightarrow \text{Fermion term} \\ & +(D_\mu\Phi)^\dagger(D^\mu\Phi) - V(\phi) && \rightarrow \text{Higgs term} \\ & -Y_{ij}\bar{\Psi}_i\Phi\Psi_j + h.c. && \rightarrow \text{Yukawa term}\end{aligned}\tag{1.1}$$

Throughout the latter half of the 20th century and through the 21st, the Standard Model has found strong agreement with many observed phenomena, while also predicting many other observables that took longer to be observed (most notably, the Higgs boson). However, there are still many observations that do not align with the Standard Model: some more large scale such as unification with gravity or a description of dark matter, some more specific such as some individual decay processes; for example, the semileptonic decay ratios $\mathcal{R}(K^{(*)})$ notoriously deviate from the Standard Model to approximately 2.5σ [2]. The modifications and additions to the Standard Model needed for these smaller scale problems could open the door to new phenomena that could bring us closer to a complete theory of nature.

1.1 The Standard Model

The Standard Model is a quantum field theory, describing all constituent particles as quantum fields permeating through space-time. There are twenty-five fundamental particles currently described in the Standard Model: twelve fermions (quarks and leptons), four gauge bosons of the electroweak theory (W^\pm, Z, γ), eight gluons of the strong force, and the Higgs boson.

The bases for the Standard Model are the quantum theories of electroweak and strong interactions, and then the symmetry-breaking Higgs mechanism which gives masses to these theories. Both the electroweak and strong theories are non-Abelian gauge theories: the electroweak theory has a gauge symmetry of $SU(2)_L \otimes U(1)_Y$, and the strong theory of $SU(3)_c$ [1, 3].¹ To formulate the Standard Model Lagrangian, we start with the free Lagrangian of a massless Dirac fermion coupled to a gauge field tensor,

$$\mathcal{L} = i\bar{\psi}\gamma^\mu\partial_\mu\psi - \frac{1}{4}F^{\mu\nu}F_{\mu\nu}. \quad (1.2)$$

The Lagrangian must be formed such that it is invariant for a local gauge transformation of the fermion field, ψ :

$$\psi(x) \rightarrow U(x)\psi(x), \quad \bar{\psi}(x) \rightarrow \bar{\psi}(x)U^\dagger(x), \quad (1.3)$$

where $U(x)$ is the gauge transformation. For $U(1)$ and $SU(N)$ symmetries, we have

$$U_{U(1)} = \exp[i\alpha], \quad U_{SU(N)} = \exp\left[i\alpha^a \frac{T^a}{2}\right]. \quad (1.4)$$

For $SU(N)$ symmetries, the index a is summed from 1 to $N^2 - 1$: this is the number of gauge fields of the group. T^a are the generators of these fields, which are represented by the Pauli matrices for $SU(2)$ and the Gell-Mann matrices for $SU(3)$. For $SU(2)$, there are three gauge fields, which will lead to the three associated bosons (W^\pm, Z) when mixed with $U(1)$; for $SU(3)$, there are eight gauge fields, leading to the eight gluons. Clearly for $U(1)$ there is only a single gauge field, which will lead to the photon when mixed with the $SU(2)$ gauge fields. In addition to the definitions in Eq.(1.4), to make Eq.(1.2) gauge invariant, it is necessary to transform the gauge field, as well as introduce the *covariant derivative*, D_μ :

$$A_\mu^a \rightarrow A_\mu^a + \frac{1}{g}\partial_\mu\alpha^a + gf^{abc}\alpha^b A_\mu^c, \quad (1.5)$$

$$\partial_\mu \rightarrow D_\mu = \partial_\mu - igT^a A_\mu^a, \quad (1.6)$$

where g is the gauge coupling parameter and f^{abc} are the structure constants defining each $SU(N)$ group; see, e.g. [4]. Note that Eqs.(1.5) and (1.6) are the general forms for the $SU(N)$ theories (when considering $U(1)$, these are simplified). The full covariant derivative of the Standard Model is

$$D_\mu = \partial_\mu - ig_1 \frac{Y}{2} B_\mu - ig_2 \frac{\sigma^i}{2} W_\mu^i - ig_3 \frac{\lambda^a}{2} G_\mu^a, \quad (1.7)$$

¹The subscripts of the symmetries describe the "charge" under which particles interact with each gauge theory: c represents the color charge of the strong force, L states that the weak force interacts only with left-handed doublets (through which the weak isospin will be defined analogous to spin), and Y represents the weak hypercharge of $U(1)$ before the spontaneous symmetry breaking of the Higgs mechanism to introduce the electric charge of the electromagnetic force; see, e.g. [4].

combining all constituent gauge groups, with $g_{1,2,3}$ the gauge coupling of $U(1)_Y$, $SU(2)_L$, and $SU(3)_c$ respectively where the gauge field(s) and generator(s) of each group are in the term of their coupling; see, e.g. [4]. From these definitions, the gauge invariance of Eq.(1.2) for $U(1)$ symmetry is trivial, and for $SU(N)$ symmetries, it will simply follow after defining a commutation relation between generators:

$$[T^a, T^b] = if^{abc}T^c, \quad (1.8)$$

As in many parts of quantum mechanics, it can be useful to define the fermion field ψ into an upper and lower part, such that ψ can be written as a linear combination of component states. This can be done in many ways, but it is important in the formulation of the Standard Model to separate the fermion field into left- and right-handed components; this was suggested in the 1950s by Lee and Yang [5] and then shown experimentally by Wu and collaborators [6], as a description of the parity violation of nature. To this end, we define the operators

$$P_L = \frac{1 - \gamma^5}{2}, \quad P_R = \frac{1 + \gamma^5}{2}, \quad (1.9)$$

where γ^5 is defined in the conventional representation. The left-handed projection of the fermion field ψ would then be

$$\psi_L = P_L \psi. \quad (1.10)$$

Now when forming the $SU(2)$ symmetry of the weak force, there is a difference between the interaction of right- and left-handed fermions: that is, left-handed fermions transform under the $SU(2)$ space, whereas right-handed do not. Considering both quarks and leptons in the traditional three generations, then under the electroweak $SU(2)$ space, each generation forms a left-handed doublet and a right-handed singlet, e.g.

$$\Psi_L = \begin{pmatrix} \nu_e \\ e^- \end{pmatrix}_L, \quad e_R^-, \quad \Psi_{L\alpha} = \begin{pmatrix} u_\alpha \\ d_\alpha \end{pmatrix}_L, \quad u_{R\alpha}, d_{R\alpha}, \quad (1.11)$$

where α represents the colour charge of the quarks under the strong interaction [4]. We can define the weak isospin quantum number T analogous to spin. In the left-handed doublet, up-type quarks and neutrinos have $T_3 = +\frac{1}{2}$, and down-type quarks and charged leptons have $T_3 = -\frac{1}{2}$. Neutrinos only appear in the left-handed doublets and do not form right-handed singlets, or if they do, these do not interact with the rest of the Standard Model. So right- and left-handed fermions are in different $SU(2)$ multiplets; this represents a parity violation in the Standard Model which is also found in nature. This is an important criterion of a theory of nature, as will be discussed more in Section 1.2.

Gauge symmetry has thus far yielded a Lagrangian to describe fermions, forces, and their interactions, but only for massless particles. This however is not observed in nature. For massive fermions and bosons, the Lagrangian would require terms of the form $m\bar{\psi}\psi$ and $m_A^2 A_\mu A^\mu$ respectively. The fermion mass term would initially seem invariant, but under the electroweak symmetry, it is rewritten as

$$m\bar{\psi}\psi = m(\bar{\psi}_R\psi_L + \bar{\psi}_L\psi_R), \quad (1.12)$$

and so is no longer invariant, due to the mixing of right-handed and left-handed spinors.

To solve this problem, the Higgs mechanism can be introduced as a way to spontaneously break the symmetry of the electroweak force to generate massive bosons [7]. The Lagrangian of the scalar Higgs reads

$$\mathcal{L} = (D^\mu \Phi)^\dagger (D_\mu \Phi) - V(\Phi). \quad (1.13)$$

Consider a complex scalar field under the SU(2) left-handed doublet representation,

$$\Phi = \frac{1}{\sqrt{2}} \begin{pmatrix} \phi_1 + i\phi_2 \\ \phi_0 + i\phi_3 \end{pmatrix} = \begin{pmatrix} \phi^+ \\ \phi^0 \end{pmatrix}, \quad (1.14)$$

which has a U(1) hypercharge $Y = +\frac{1}{2}$ [7]. The covariant derivative in Eq.(1.13) is that defined for SU(2)⊗U(1):

$$D_\mu \phi = \left(\partial_\mu + igT^i W_\mu^i + \frac{i}{2}g'B_\mu \right) \phi, \quad (1.15)$$

with W_μ^i and B_μ the gauge fields of SU(2)_L and U(1)_Y, and g and g' the SU(2) and U(1) gauge couplings respectively. The Higgs potential $V(\Phi)$ in Eq.(1.13) is defined as

$$V(\phi) = -\mu^2 \Phi^\dagger \Phi + \lambda(\Phi^\dagger \Phi)^2. \quad (1.16)$$

If $\mu^2 > 0$, then the scalar field will acquire a non-zero vacuum expectation value (VEV), which will spontaneously break the symmetry. The VEV can be defined as

$$\langle \Phi \rangle = \frac{1}{\sqrt{2}} \begin{pmatrix} 0 \\ v \end{pmatrix}. \quad (1.17)$$

To ensure that the symmetry of electromagnetism is not broken, the scalar field ϕ^0 is taken to have charge $Q = 0$. Under this scheme, both the hypercharge Y and the weak isospin T_3 are not conserved, but the specific combination of them which is defined as electric charge, $Q = T_3 + \frac{1}{2}Y$ is conserved, so the electroweak symmetry is spontaneously broken to form a U(1) symmetry of electric charge Q ,

$$SU(2)_L \otimes U(1)_Y \rightarrow U(1)_Q. \quad (1.18)$$

The W^\pm and Z masses can now be generated from this mechanism. In the unitary gauge, the scalar doublet can be written

$$\Phi = \frac{1}{\sqrt{2}} \begin{pmatrix} 0 \\ v + h \end{pmatrix}. \quad (1.19)$$

Through substituting the above into Eq.(1.13), the gauge fields of the real electroweak bosons W^\pm , Z , γ can be found as linear combinations of W_μ^i and B_μ with their mass terms now generated in a gauge invariant form:

$$W_\mu^\pm \equiv \frac{1}{\sqrt{2}}(W_\mu^1 \mp iW_\mu^2), \quad m_W = \frac{gv}{2}, \quad (1.20)$$

$$Z_\mu \equiv \frac{1}{\sqrt{g^2 + g'^2}}(gW_\mu^3 - g'B_\mu), \quad m_Z = \frac{v}{2}\sqrt{g^2 + g'^2}, \quad (1.21)$$

$$A_\mu \equiv \frac{1}{\sqrt{g^2 + g'^2}}(g'W_\mu^3 + gB_\mu), \quad m_A = 0. \quad (1.22)$$

It can be said that three of the component scalar fields in Eq.(1.14) were "eaten" to form the gauge boson masses, and the fourth field becomes the Higgs boson [7].

Now the final piece of the puzzle is fermion masses. We consider the final term of Eq.(1.1), the Yukawa Lagrangian. It is split into two terms: the one written and "h.c.", representing the hermitian conjugate of the former. The hermitian conjugate term is required so both up-type quarks, and down-type quarks and charged leptons gain mass [7]. In the unitary gauge, the down-type quark Yukawa term reads

$$-\mathcal{L}_{Yuk}^d = \sum_{a,b} Y_{ab}^{(d)} (\bar{u}_{aL} \bar{d}_{aL}) \begin{pmatrix} 0 \\ \frac{v}{\sqrt{2}} \end{pmatrix} d_{bR} = \sum_{a,b} Y_{ab}^{(d)} \phi_0 \bar{d}_{aL} d_{bR}, \quad (1.23)$$

where ϕ^0 is defined as $\frac{v}{\sqrt{2}}$ through the transformation

$$\Phi = \frac{1}{\sqrt{2}} \begin{pmatrix} 0 \\ v+h \end{pmatrix} \rightarrow \frac{1}{\sqrt{2}} \begin{pmatrix} 0 \\ v \end{pmatrix} \quad (1.24)$$

from the spontaneous symmetry breaking. So now down-type quarks have gained masses. To generate the masses of the up-type quarks, the hermitian conjugate term is used, where now a second Higgs doublet (not independent of the first, but its charge conjugate) is introduced as

$$\tilde{\Phi} = i\sigma_2 \Phi^* = \begin{pmatrix} \phi^{0*} \\ -\phi^{+*} \end{pmatrix} = \frac{1}{\sqrt{2}} \begin{pmatrix} v+h \\ 0 \end{pmatrix}. \quad (1.25)$$

The up-type quark Yukawa term is then

$$-\mathcal{L}_{Yuk}^u = \sum_{a,b} Y_{ab}^{(u)} (\bar{u}_{aL} \bar{d}_{aL}) \begin{pmatrix} \frac{v}{\sqrt{2}} \\ 0 \end{pmatrix} u_{bR} = \sum_{a,b} Y_{ab}^{(u)} \phi^0 \bar{u}_{aL} u_{bR}. \quad (1.26)$$

The charged lepton masses are generated similarly to the down-type quarks, and the expressions of masses read

$$m_i = -\frac{Y_i v}{\sqrt{2}}, \quad (1.27)$$

where i will represent the fermions; see, e.g. [4]. The question of neutrino mass is at the forefront of some research, and so will not be mentioned in this study, other than that it is now known that neutrinos do have mass, however small.

In Eqs.(1.23) and (1.26), we have formed what may be non-diagonal mass matrices. These can be diagonalised in which the constituent states are the mass eigenstates, e.g. for the quarks, there would be

$$\frac{v}{\sqrt{2}} V_1^\dagger Y_u V_1 = \begin{pmatrix} m_u & & \\ & m_c & \\ & & m_t \end{pmatrix}, \quad \frac{v}{\sqrt{2}} V_2^\dagger Y_d V_2 = \begin{pmatrix} m_d & & \\ & m_s & \\ & & m_b \end{pmatrix}. \quad (1.28)$$

It may or may not be possible for these matrices to be diagonalised simultaneously, however, this is not generally expected so we do not start under any assumption. By convention, it is chosen to diagonalise the up-type quarks, and then rotate the down-type quarks

between their weak eigenstates and their mass eigenstates [8]. The famous Cabibbo-Kobayashi-Maskawa (CKM) matrix, defined $V_{CKM} \equiv V_1^\dagger V_2$, is the matrix connecting mass and weak eigenstates,

$$\begin{pmatrix} d \\ s \\ b \end{pmatrix} = V_{CKM} \begin{pmatrix} d' \\ s' \\ b' \end{pmatrix}, \quad (1.29)$$

as well as describing quark mixing between the up- and down-type quarks [9]. The CKM matrix in its full form is a unitary matrix; within the SM, it is a 3×3 unitary matrix. In principle it could be a section of a 4×4 unitary matrix if a fourth generation of fermions existed, meaning the current 3×3 matrix would not necessarily be unitary. The strengths of quark coupling are stored in elements of the CKM matrix as

$$V_{CKM} = \begin{pmatrix} V_{ud} & V_{us} & V_{ub} \\ V_{cd} & V_{cs} & V_{cb} \\ V_{td} & V_{ts} & V_{tb} \end{pmatrix}. \quad (1.30)$$

These individual elements can be found through quark coupling processes. For better understanding of the CKM matrix, however, it can be easier to parameterise it. The two most common parameterisations are the *standard parameterisation* [2], which is exact, and the *Wolfenstein parameterisation*, which is an approximation [10]. The standard parameterisation follows from extension of the Cabibbo angle for mixing between the first and second generations [11], where we now use three Cabibbo-like matrices for interactions of two generations, and include a phase required by the formation of a 3×3 unitary matrix:

$$\begin{aligned} V_{CKM} &= \begin{pmatrix} 1 & 0 & 0 \\ 0 & \cos \theta_{23} & \sin \theta_{23} \\ 0 & -\sin \theta_{23} & \cos \theta_{23} \end{pmatrix} \begin{pmatrix} \cos \theta_{13} & 0 & \sin \theta_{13} e^{i\delta} \\ 0 & 1 & 0 \\ -\sin \theta_{13} e^{i\delta} & 0 & \cos \theta_{13} \end{pmatrix} \begin{pmatrix} \cos \theta_{12} & \sin \theta_{12} & 0 \\ -\sin \theta_{12} & \cos \theta_{12} & 0 \\ 0 & 0 & 1 \end{pmatrix} \\ &= \begin{pmatrix} c_{12}c_{13} & s_{12}c_{13} & s_{13}e^{-i\delta} \\ -s_{12}c_{23} - c_{12}s_{23}s_{13}e^{i\delta} & c_{12}c_{23} - s_{12}s_{23}s_{13}e^{i\delta} & s_{23}c_{13} \\ s_{12}c_{23} - c_{12}c_{23}s_{13}e^{i\delta} & -c_{12}s_{23} - s_{12}c_{23}s_{13}e^{i\delta} & c_{23}c_{13} \end{pmatrix}. \end{aligned} \quad (1.31)$$

The Wolfenstein parameterisation approximates the standard parameterisation as $\lambda = s_{12} \approx 0.224834$, $A\lambda^2 = s_{23}$, and $A\lambda^3(\rho - i\eta) = s_{13}e^{-i\delta}$, and performs a Taylor expansion traditionally to order λ^3 to yield

$$V_{CKM} = \begin{pmatrix} 1 - \frac{\lambda^2}{2} & \lambda & A\lambda^3(\rho - i\eta) \\ -\lambda & 1 - \frac{\lambda^2}{2} & A\lambda^2 \\ A\lambda^3(1 - \rho - i\eta) & -A\lambda^2 & 1 \end{pmatrix} + \mathcal{O}(\lambda^4). \quad (1.32)$$

This parameterisation makes it very easy to see the relative strengths of the couplings.

An important element of the CKM matrix is its complex phase.² The presence of a complex phase allows for CP-violating processes to take place in the Standard Model: the CKM matrix's hermitian conjugate will give the complex conjugated phase, yielding different physics over CP conjugation for complex coupling elements. In the Wolfenstein

²If it were a 4×4 matrix, there would be three phases, implying significantly more CP violation.

parameterisation, all CP violation is held with the $i\eta$ terms. Plotting measurements in the (ρ, η) plane can prove useful in understanding these terms, to which end the unitarity triangle can be formed:

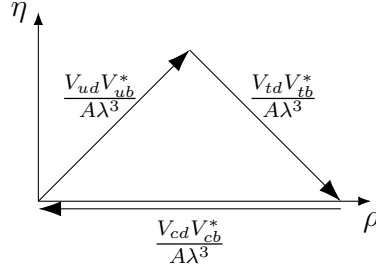


Figure 1: The unitarity triangle from the Wolfenstein parameterisation in (ρ, η) space.

The unitarity triangle can help describe many things in quark mixing, such as CP violation, through the length of its side and its angles. Through comparison of experiment and theory in CP-violating processes, many regions in the (ρ, η) plane can be defined to work as a consistency check of the SM and describe various effects in quark mixing.

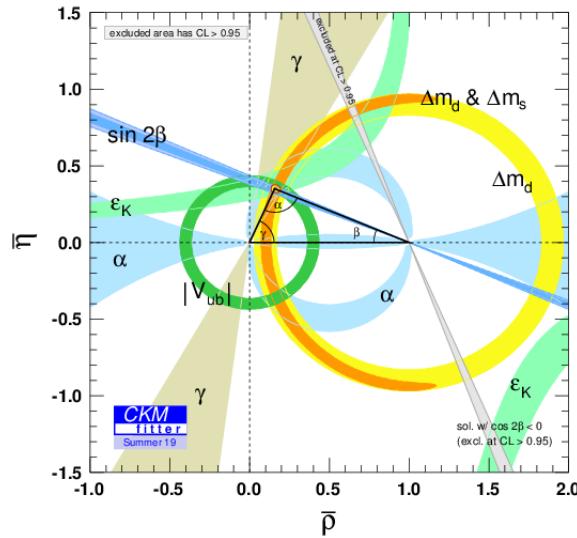


Figure 2: The global CKM fit in the (ρ, η) plane, as of 17/04/20 [12].

1.2 Flavour Physics and CP Violation

One of the big questions about the formulation of our universe is why is there an asymmetry between matter and anti-matter, known as Baryogenesis. Sakharov stated in 1967 three criteria that must have been fulfilled throughout the evolution of the Universe to create the current state of matter-antimatter asymmetry [13]. These are:

1. Baryon Number Violation - this is theorised in sphalerons, though not yet confirmed experimentally [14].
2. C and CP Violation - this is present in the Standard Model, although not to the extent required.

3. A First Order Phase Transition in the early universe - this could have been possible in the Standard Model, but only for $m_h \lesssim 70 \text{ GeV}$ [15], whereas we now measure the Higgs mass to be $m_h = 125.1 \pm 0.14 \text{ GeV}$ [2].

A significant focus of flavour physics is the study of CP violation - the violation of CP symmetry (the product of Charge and Parity symmetries) in the Standard Model. CP symmetry was introduced as a candidate for the fundamental symmetry of Standard Model interactions after Parity violation was discovered in 1957 [6]. Not long after, CP violation was also discovered, in 1964 in Kaon mixing [16]. CP violation has since been studied in the b-quark sector (see e.g. [17]) and recently discovered as well in the c-quark sector [18]. The necessity of CP violation for the question of baryogenesis is apparent: if left-handed baryons interact differently to right-handed anti-baryons, then one of these can be more prominent than the other. Both the electromagnetic and strong forces appear to conserve CP, the weak force, however, through the chiral nature of its couplings, does not. There are two ways for CP-violating interactions to occur through the weak force: through complex Yukawa couplings in the CKM matrix; and through complex Higgs parameters, such as those in the Two Higgs Doublet Models to be discussed in Section 1.3. There is also a question of whether CP violation can be found in the strong sector, but this will not be discussed here.

Currently, there is a significant crux to the study of Sakharov's condition of CP violation: the amount of CP violation currently observed would not be enough to account for the large baryon asymmetry of the universe. This points toward physics beyond the Standard Model to add to the CP violation predicted and perhaps predict where to observe the CP violation needed in nature. There are many proposals for Standard Model extensions which could bridge the gap between theory and experiment, although these extensions would require new particles and processes to explain their phenomena, none of which have so far been observed.

The Z' boson, for example, is a common extension to the Standard Model, which in its simplest application behaves akin to the Z^0 boson but with a higher mass. There are many descriptions of the Z' boson ranging from the introduction of a new U(1) gauge symmetry to the inclusion of string theory; for a review, see [19].

It could also be possible that there is a fourth generation of fermions, perfectly replicating the first generation to higher masses as the second and third generations do. The presence of the fourth generation could add extra Feynman diagrams to decays, increasing the resulting decay amplitude. Another interesting implication of a fourth generation would be that the CKM matrix would now be a 4×4 matrix, which could see some alterations to flavour-changing interactions, even some additional complex terms where CP violation would arise. A key indicator on this extension is in the Higgs mechanism.

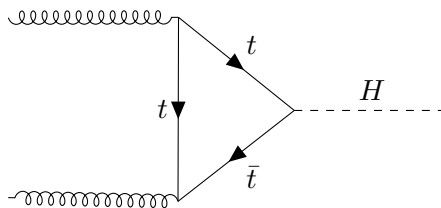


Figure 3: Higgs boson production through the top quark loop.

The Higgs couples more strongly to heavier particles, so the top-Higgs vertex seen in Figure 3 should be replicated with the theoretical t' and b' quarks with increased amplitudes. However, when just considering the SM4 model, the new prediction of the Higgs scattering amplitude is far greater than that observed [20]. It could be possible that the SM4 model is physical, but would also need another extension to resolve its issues, such as the Two Higgs Doublet Model discussed below [21].

Whenever constructing new theories to extend the Standard Model, inspiration can frequently come from a few specific cases of anomaly which hint to new physics. However, it is important to test these extensions across all observables which could involve the new processes. If the extension resolves issues with some observables while creating new ones with others, then it is of no use; only extensions which work across the whole spectrum of phenomena (as well as, or better than, the SM) can be physical.

1.3 The Two Higgs Doublet Model of Type II

First, it is important to specify what makes the 2HDM Type II an interesting New Physics model to study. As hinted at when discussing the Sakharov criteria, one way of inducing CP violation would be through complex Higgs parameters. There are no such complex parameters in the Higgs sector of the Standard Model, however, as shown above, these are apparent in the 2HDM, and therefore we can introduce additional CP violation to possibly meet Sakharov's criterion. In addition to increased CP violation, the 2HDM also solves the problem of Sakharov's third criterion: under this model, a first order phase transition is present for $m_h = 125$ GeV.

There is also the possibility that this model can resolve the issues of a fourth generation of fermions, under certain criteria. This is discussed later in Section 2.6.

Previously in the Standard Model Higgs mechanism, to generate the masses of the weak gauge bosons and fermions, a single Higgs SU(2) doublet of complex scalar fields was introduced, as in Eq.(1.14). To form masses for both up- and down-type quarks and charged leptons, we introduced the hermitian conjugate doublet in Eq.(1.25), otherwise the Higgs field would only give mass to the down-type quarks and charged leptons. Now two independent Higgs doublets can be postulated, of the general form

$$\Phi_1 = \begin{pmatrix} \phi_1 + i\phi_2 \\ \phi_0 + i\phi_3 \end{pmatrix}, \quad \Phi_2 = \begin{pmatrix} \phi_5 + i\phi_6 \\ \phi_4 + i\phi_7 \end{pmatrix}. \quad (1.33)$$

These two doublets would have opposite hypercharge so one would couple to up-type quarks, and the other to down-type [22]. Each doublet would have its own VEV, with the quadrature addition of these two VEVs creating the value measured in experiment:

$$\Phi_1 = \frac{1}{\sqrt{2}} \begin{pmatrix} 0 \\ v_1 \end{pmatrix}, \quad \Phi_2 = \frac{1}{\sqrt{2}} \begin{pmatrix} v_2 \\ 0 \end{pmatrix}, \quad v_{SM}^2 = v_1^2 + v_2^2. \quad (1.34)$$

In this model, the masses of the three weak gauge bosons can still be generated in the same way, each eating one of the scalar fields. This time, however, there would be 5 residual scalar fields, and so, five Higgs fields should be found: three neutral Higgs - two scalar H^0 and h^0 (where h^0 is the SM Higgs particle) and one pseudoscalar A^0 . There will also be two charged Higgs H^\pm . The introduction of these new particles requires searching for

additional parameters to describe them: the masses of H^0 , A^0 , and H^\pm ; the mixing angle between h^0 and H^0 , α ; and the VEV ratio $\tan\beta = v_2/v_1$ [23]. The two Higgs doublet model (2HDM) potential can be written in its most general form as

$$V(\Phi_1, \Phi_2) = m_{11}^2 \Phi_1^\dagger \Phi_1 + m_{22}^2 \Phi_2^\dagger \Phi_2 + m_{12}^2 (\Phi_1^\dagger \Phi_2 + \Phi_2^\dagger \Phi_1) + \frac{\lambda_1}{2} (\Phi_1^\dagger \Phi)^2 + \frac{\lambda_2}{2} (\Phi_2^\dagger \Phi_2)^2 \\ + \lambda_3 \Phi_1^\dagger \Phi_1 \Phi_2^\dagger \Phi_2 + \lambda_4 \Phi_1^\dagger \Phi_2 \Phi_2^\dagger \Phi_1 + \frac{\lambda_5}{2} \left[(\Phi_1^\dagger \Phi_2)^2 + (\Phi_2^\dagger \Phi_1)^2 \right]. \quad (1.35)$$

The 2HDM described above is the type II version, where Φ_1 couples to up-type quarks and Φ_2 couples to down-type quarks and charged leptons. There are other types of 2HDM where the two Higgs doublets couple in different ways, but the comforting sign from Type II is that it yields a similar expression for the Yukawa Lagrangian to the SM; see, e.g. [23]. This in turn yields a similar CKM matrix through which all flavour-changing interactions can be described. The addition of 4 new Higgs fields introduces new interactions, where the charged Higgs fields can replace W^\pm fields in flavour-changing charged interactions, as well as additional neutral interactions between the neutral Higgs scalar and pseudoscalar fields [22].

The charged Higgs particles can mediate weak charged currents in the same way as W^\pm , and the additional contribution of H^\pm to many weak-mediated decays could correct the Standard Model to predict these decay paths more accurately to experiment [22]. The important factors to determine whether these charged Higgs could be the answer to the inconsistencies are the relevant parameters from the 2HDM: the charged Higgs mass m_{H^\pm} , and the VEV ratio $\tan\beta$ [24]. Values of these parameters which align theory and observation can indicate where LHC experiments could probe for these theorised new particles. This study considers where regions of the 2HDM Type II parameters can align SM predictions with experiment, giving indication of where they could be found in nature if this model is to be a real extension of the Standard Model.

2 Probing the 2HDM Type II

As mentioned previously, the 2HDM is easy to probe through the charged weak current, where interactions will gain additional pathways replacing a W^\pm with a H^\pm . Studies of these new contributions have been done in the past, though it is interesting to revisit this now as new measurements have been performed, and SM calculations become more precise. For flavour observables, a study of the most relevant decays for charged Higgs searches was done in [24]. Here, we begin by following [24] closely to find the changes to their results in the last ten years, before moving on to further additions. The up-to-date measurements and parameters used for these expressions are given in Tables 1 and 2. For parameters in these expressions not quoted in the tables, we use [12] for the CKM elements, and [2] for all else, such as the quark masses and meson lifetimes.

2.1 Leptonic Decays

Following [24], the Standard Model leptonic decay $M \rightarrow l\nu_l$, where M is a charged meson, has a branching ratio of

Observable	Value	Unit	Reference
$\Gamma[K^+ \rightarrow \mu^+ \nu_\mu]/\Gamma[\pi^+ \rightarrow \mu^+ \nu_\mu]$	1.337 ± 0.003		[2]
$\Gamma[\tau^+ \rightarrow K^+ \nu_\tau]/\Gamma[\tau^+ \rightarrow \pi^+ \nu_\tau]$	6.438 ± 0.094	10^{-2}	[2]
$\mathcal{B}r[B^+ \rightarrow \mu^+ \nu_\mu]$	5.3 ± 2.2	10^{-7}	[30]
$\mathcal{B}r[B^+ \rightarrow \tau^+ \nu_\tau]$	1.09 ± 0.24	10^{-4}	[2]
$\mathcal{B}r[D^+ \rightarrow \mu^+ \nu_\mu]$	3.82 ± 0.33	10^{-4}	[2]
$\mathcal{B}r[D_s^+ \rightarrow \mu^+ \nu_\mu]$	5.52 ± 0.16	10^{-3}	[2]
$\mathcal{B}r[D_s^+ \rightarrow \tau^+ \nu_\tau]$	5.48 ± 0.23	10^{-2}	[2]
$\mathcal{B}r[\bar{B} \rightarrow X_s \gamma]$	3.32 ± 0.15	10^{-4}	[31]
$\mathcal{B}r[\bar{B} \rightarrow X_c e \bar{\nu}]$	10.65 ± 0.16	10^{-2}	[2, 31]
$\mathcal{B}r[\bar{B} \rightarrow X_u e \bar{\nu}]$	8.41 ± 0.59	10^{-4}	[32]
$\mathcal{B}r[B_d \rightarrow \mu^+ \mu^-]$	$1.4^{+1.6}_{-1.4}$	10^{-10}	[2]
$\mathcal{B}r[B_s \rightarrow \mu^+ \mu^-]$	3.1 ± 0.7	10^{-9}	[31]
Δm_d	0.5064 ± 0.0019	ps^{-1}	[31]
Δm_s	17.757 ± 0.021	ps^{-1}	[31]
$\mathcal{R}(D)$	0.340 ± 0.030		[31]
$\mathcal{R}(D^*)$	0.298 ± 0.014		[31]
S	0.02 ± 0.10		[2]
T	0.07 ± 0.12		[2]
U	0.00 ± 0.09		[2]

Table 1: Updated branching ratios and other observables used in testing parameter space of 2HDM Type II. In the case of normalised ratios, values have been calculated using the constituent measurements taken from reference.

$$\mathcal{B}r[M \rightarrow l \nu_l]_{\text{SM}} = \frac{G_F^2 m_M m_l^2}{8\pi} \left(1 - \frac{m_l^2}{m_M^2}\right)^2 |V_{quqd}|^2 f_M^2 \tau_M (1 + \delta_{EM}^{Ml2}), \quad (2.1)$$

where q_u and q_d represent the up- and down-like quarks of the meson, V_{quqd} the CKM element, f_M the M meson's decay constant, τ_M the meson lifetime, and G_F is the Fermi constant, defined as

$$G_F = \frac{g_2^2 \sqrt{2}}{8M_W^2} \approx 1.166 \times 10^{-5} \text{ GeV}^{-2} [2]. \quad (2.2)$$

δ_{EM}^{Ml2} is a corrective factor for electromagnetic radiative corrections [2]. For π and K mesons, the effect is around 2-3% and around 1% for D mesons. For B meson phenomena, the effect is approximated to 0. For the light mesons, kaons and pions, it is easier to determine the ratio of their decay constants f_K/f_π than the individual values. Thus, it is then easier to consider the ratio of their branching fractions. In the Standard Model,

$$\frac{\Gamma[K \rightarrow \mu \nu]_{\text{SM}}}{\Gamma[\pi \rightarrow \mu \nu]_{\text{SM}}} = \frac{m_K}{m_\pi} \left(\frac{1 - m_l^2/m_K^2}{1 - m_l^2/m_\pi^2} \right)^2 \left| \frac{V_{us}}{V_{ud}} \right|^2 \left(\frac{f_K}{f_\pi} \right)^2 (1 + \delta_{EM}^{Kl2/\pi l2}). \quad (2.3)$$

It is also worth considering the ratio of tau decays of kaons to pions:

$$\frac{\Gamma[\tau \rightarrow K \nu]_{\text{SM}}}{\Gamma[\tau \rightarrow \pi \nu]_{\text{SM}}} = \left(\frac{1 - m_K^2/m_\tau^2}{1 - m_\pi^2/m_\tau^2} \right)^2 \left| \frac{V_{us}}{V_{ud}} \right|^2 \left(\frac{f_K}{f_\pi} \right)^2 (1 + \delta_{EM}^{\tau K2/\tau \pi 2}). \quad (2.4)$$

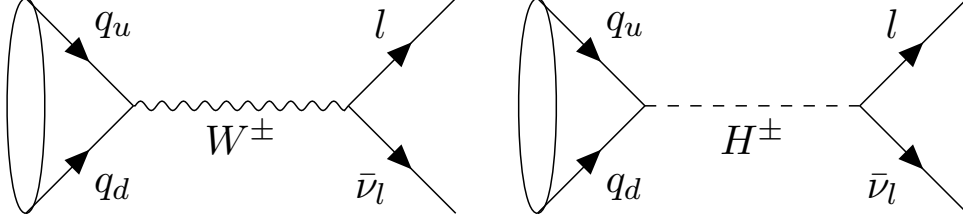


Figure 4: W^\pm and H^\pm pathways for the leptonic decay of a meson (before higher-order terms).

These SM branching values will take alterations from the two Higgs doublet model of the form

$$\mathcal{B}r[M \rightarrow l\nu] = \mathcal{B}r[M \rightarrow l\nu]_{\text{SM}}(1 + r_H)^2, \quad (2.5)$$

where r_H is the corrective factor of the two Higgs doublet model:

$$r_H = \left(\frac{m_{q_u} - m_{q_d} \tan^2 \beta}{m_{q_u} + m_{q_d}} \right) \left(\frac{m_M}{m_{H^\pm}} \right)^2. \quad (2.6)$$

It can still be possible through this method for some leptonic decays to have agreement between the SM predictions and experiment, where $r_H = 0, -2$. $r_H = 0$ is known as the decoupling solution which can be found as m_{H^\pm} approaches infinity; $r_H = -2$, the fine-tuned solution, is obtained from a linear relationship between m_{H^\pm} and $\tan \beta$, which will be dependent of the masses of the meson and its constituent quarks, so will vary between mesons.

2.2 Mass mixing

Neutral B meson mixing is a common focus in flavour physics, due to the strong dependence on the heavy W exchange. A key observable in the study of B-mixing is the mass

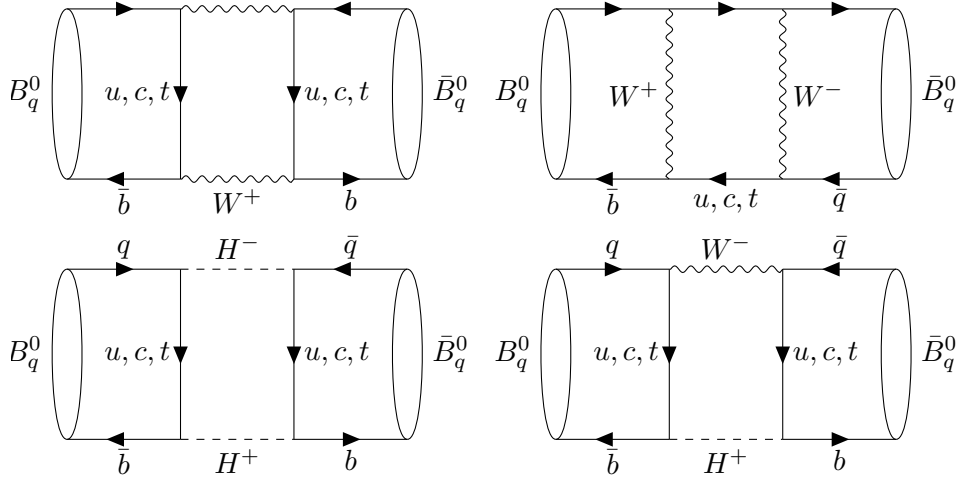


Figure 5: Examples of the box diagrams detailing B_d and B_s meson mixing.

difference Δm_q between the two mass eigenstates, $\Delta m_q = M_H^q - M_L^q$, where ‘ H ’ denotes the ‘heavy’ eigenstate and ‘ L ’ denotes the ‘light’. A thorough description of this process can be found, for example, in [17]. In the 2HDM, the mass difference receives two additional contributions from box diagrams using the heavy charged Higgs in place of both

W s or one W . Following [25] for B_q , where $q = d, s$, this results (to Leading Order) in:

$$\Delta m_q = \frac{G_F^2}{6\pi^2} (V_{tq} V_{tb}^*)^2 \hat{\eta}_B m_B m_W^2 f_{B_q}^2 B_{B_q} (S_{WW} + 2S_{WH} + S_{HH}), \quad (2.7)$$

$$S_{WW} = x_{tW} \left(\frac{1}{4} + \frac{9}{4(1-x_{tW})} - \frac{3}{2(1-x_{tW})^2} - \frac{3x_{tW}^2 \ln(x_{tW})}{2(1-x_{tW})^3} \right), \quad (2.8)$$

$$S_{HH} = \frac{x_{tH} x_{tW}}{4 \tan^4 \beta} \left(\frac{1+x_{tH}}{(1-x_{tH})^2} + \frac{2x_{tH} \ln(x_{tH})}{(1-x_{tH})^3} \right), \quad (2.9)$$

$$2S_{WH} = \frac{x_{tH} x_{tW}}{4 \tan^2 \beta} \left(\frac{(2x_{tW} - 8x_{tH}) \ln(x_{tH})}{(1-x_{tH})^2 (x_{tH} - x_{tW})} + \frac{6x_{tW} \ln(x_{tW})}{(1-x_{tW})^2 (x_{tH} - x_{tW})} - \frac{8 - 2x_{tW}}{(1-x_{tH})(1-x_{tW})} \right). \quad (2.10)$$

where $x_{ij} = m_i^2/m_j^2$, and S_{xy} describes the internal bosonic lines for the two bosons $x, y \in H^\pm, W^\pm$. These expressions are accurate for $\tan \beta \ll \frac{m_t}{m_b}$ in the 2HDM Type II. The more accurate Next-to-Leading-Order (NLO) expressions in the 2HDM are also found in [25], but these could not be included due to time restrictions. The current SM predictions are stated in [26] as

$$\Delta m_d^{\text{SM}} = (0.533_{-0.036}^{+0.022}) ps^{-1} = (1.05_{-0.07}^{+0.04}) \Delta m_d^{\text{exp}}, \quad (2.11)$$

$$\Delta m_s^{\text{SM}} = (18.4_{-1.2}^{+0.7}) ps^{-1} = (1.04_{-0.07}^{+0.04}) \Delta m_s^{\text{exp}}. \quad (2.12)$$

2.3 Radiative decay

The radiative decay $b \rightarrow s\gamma$ occurs through the flavour-changing neutral currents of penguin diagrams. The Standard Model calculations of $\bar{B} \rightarrow X_s \gamma$ have been performed up to Next-to-Next Leading Order (NNLO) [27], which yields a complicated expression, so the result is parameterised in line with [24, 28].

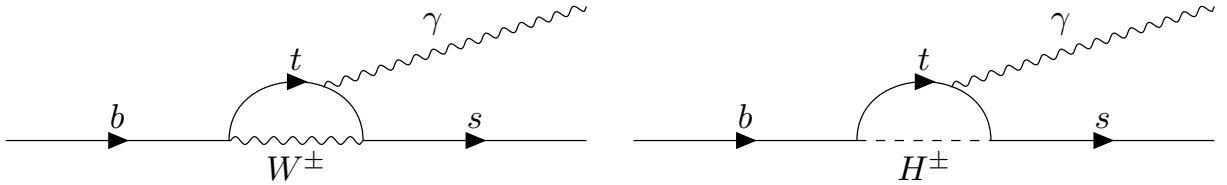


Figure 6: One-loop penguin diagrams for $b \rightarrow s\gamma$ decay.

Similarly to B meson mixing, we can substitute W^\pm for H^\pm in the relevant penguin diagrams, giving extra contributions again to the theory. The 2HDM corrections given by these additional contributions are calculated to NLO in [28], so the SM parameters must be limited to NLO. The branching ratio of $\bar{B} \rightarrow X_s \gamma$ is given by

$$\mathcal{Br}[\bar{B} \rightarrow X_s \gamma] = \mathcal{Br}[\bar{B} \rightarrow X_c l \bar{\nu}] \left| \frac{V_{ts}^* V_{tb}}{V_{cb}} \right|^2 \frac{6\alpha_{\text{EM}}}{\pi C} (P + N), \quad (2.13)$$

where we calculate using the branching ratio of $\bar{B} \rightarrow X_c l \bar{\nu}$ to cancel out the high uncertainties from quark mass terms. Here, P represents the perturbative leading contribution in the heavy quark expansion, and N the non-perturbative higher-order contributions of the heavy quark expansion. P and N are parameterised in [24, 28] as

$$P + N = (C_{7,SM}^{\text{eff},(0)} + B\Delta C_{7,H^\pm}^{\text{eff},(0)})^2 + A, \quad (2.14)$$

Input	Value	Unit	Reference
Decay Constants			
f_K/f_π	1.1932 ± 0.0019		[2]
f_B	190 ± 1.3	MeV	[33]
f_{B_s}	230 ± 1.3	MeV	[33]
f_D	212 ± 0.7	MeV	[33]
f_{D_s}	249.9 ± 0.5	MeV	[33]
Radiative corrections			
$\delta_{EM}^{Kl2/\pi l2}$	-0.0069 ± 0.0017		[2]
$\delta_{EM}^{\tau K2/\tau \pi 2}$	0.003		[24]
B meson mixing			
$f_{B_d}^2 B_{B_d}$	0.0305 ± 0.0011	GeV ²	[26]
$f_{B_s}^2 B_{B_s}$	0.0452 ± 0.0014	GeV ²	[26]
$\hat{\eta}_B$	0.838606		[34]
$\mathbf{b} \rightarrow \mathbf{s} \gamma$ parameters			
m_t^{pole}	172.9 ± 0.4	GeV	[2]
$\alpha_S(m_Z)$	0.1179 ± 0.001		[2]
μ_b	1.095	GeV	

Table 2: Parameters used in the 2HDM fits for decays outlined in Section 2.

where A and B are functions defined in Appendix B of [24], $C_{7,SM}^{\text{eff},(0)}$ is one of the Wilson coefficients of the effective Hamiltonian in the SM, and $\Delta C_{7,H^+}^{\text{eff},(0)}$ holds the charged Higgs contributions to the SM Wilson coefficient. Although these expressions are calculated to NLO, in calculating the above Wilson coefficients, we choose a renormalisation scheme μ_b such that we recover the results of the NNLO calculation.

In Eq.(2.13), C is the non-perturbative phase-space normalisation factor for the difference between the charmed semileptonic branching ratio and $\bar{B} \rightarrow X_s \gamma$. From [27], it is defined as

$$C = \left| \frac{V_{ub}}{V_{cb}} \right|^2 \frac{\Gamma(\bar{B} \rightarrow X_c e \bar{\nu})}{\Gamma(\bar{B} \rightarrow X_u e \bar{\nu})}. \quad (2.15)$$

This factor is important to cancel out the charm contribution we included earlier in $\mathcal{B}r[\bar{B} \rightarrow X_c l \bar{\nu}]$ to return us to the charmless state we consider. For these calculations, we follow the parameterisation of this process laid out in Appendix B of [24].

2.4 Updating The 2HDM Constraints

Before updating and expanding on the fit performed in [24], we check that we can replicate their results from 2009 and update this with the most recent input values. All processes mentioned above were used to test the constraints on the 2HDM parameters m_{H^+} and $\tan \beta$. The 2HDM-extended branching ratios were tested in $(m_{H^+}, \tan \beta)$ parameter space to search for regions where a charged Higgs would be allowed by nature. The individual

constraints found for leptonic decays, B meson mixing, and the radiative $b \rightarrow s\gamma$ decay are shown in Figure 7 in a log-log scale. After the constraints on the 2HDM for each individual process were found, they were combined for a global fit shown in Figure 8b (again in a log-log scale), yielding an overall allowed region in $(m_{H^+}, \tan\beta)$ space.

For each constraint, a scan was performed to 2σ to find regions where the parameter space is not excluded at this level. A χ^2 fit was then performed to constrain these regions to where $\Delta\chi^2$ corresponded to 95% CL exclusion, such that each coloured region shown in these figures shows what is not excluded to 95% CL. For the combined fit, we also show the 1σ confidence region.

To test the validity of these results, we also show what our calculations produce for 2009 inputs, as done in [24]. This fit is shown in Figure 8a, where it is seen to replicate the previous results, finding $m_{H^+} > 316$ GeV at 95% CL. The 2HDM is generally taken to

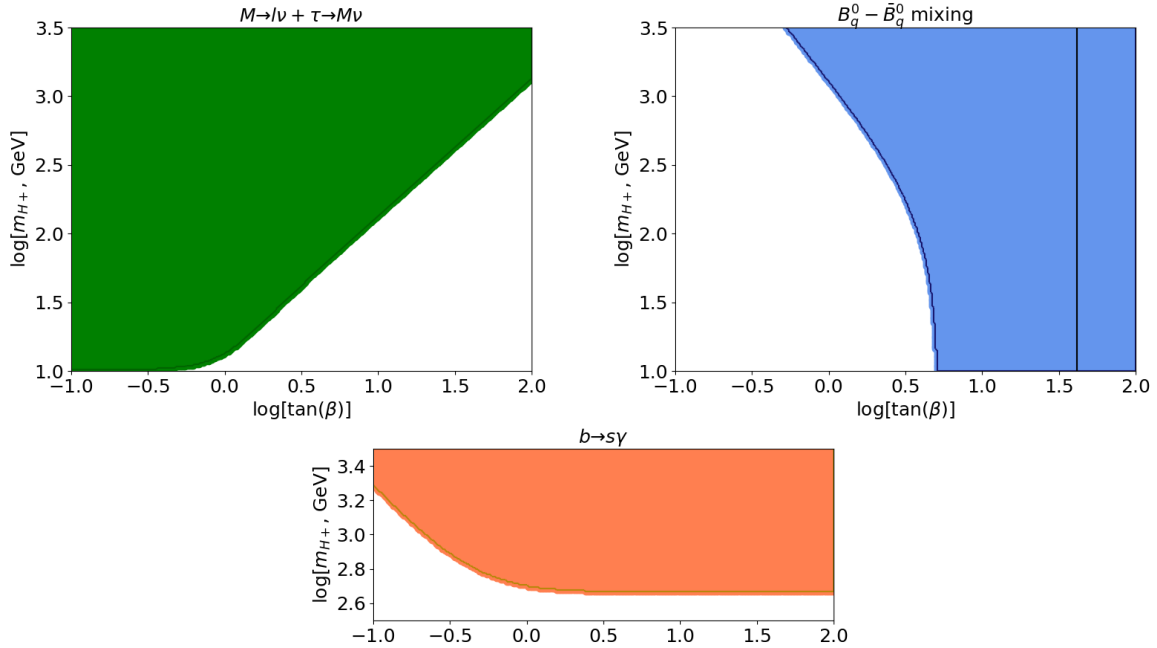


Figure 7: Constraints of $(m_{H^+}, \tan\beta)$ space from leptonic decays (top left), B_d and B_s mixing (top right), and the radiative $b \rightarrow s\gamma$ decay (bottom). The leptonic decays used were $B^+ \rightarrow \tau^+\nu$, $B^+ \rightarrow \mu^+\nu$, $D^+ \rightarrow \mu^+\nu$, $D_s^+ \rightarrow \mu^+\nu$, $D_s^+ \rightarrow \tau^+\nu$, and the ratios $K \rightarrow \mu\nu/\pi \rightarrow \mu\nu$ and $\tau \rightarrow K\nu/\tau \rightarrow \pi\nu$. The solid black vertical line (top right) shows $\tan\beta = m_t/m_b$, as for $\tan\beta$ much greater than this, the formulae for B mixing become invalid. Each region shows what is not excluded to 95% CL, as discussed in the text.

be a decoupling theory. That is, taking the limit $m_{H^+} \rightarrow \infty$ should recover the Standard Model picture of physics. For as far as we scan here, this is reinforced in our results, such that there is no upper bound on m_{H^+} . We also see that for the combined fit, $\tan\beta$ will extend both to smaller and larger values as $m_{H^+} \rightarrow \infty$, such that there is no definitive constraint on $\tan\beta$. There is, however, a clear indication of a minimum allowed value for m_{H^+} , found here as

$$m_{H^+} > \begin{array}{l} 480 \text{ GeV, } 95\% \text{ CL,} \\ 750 \text{ GeV, } 1\sigma. \end{array} \quad (2.16)$$

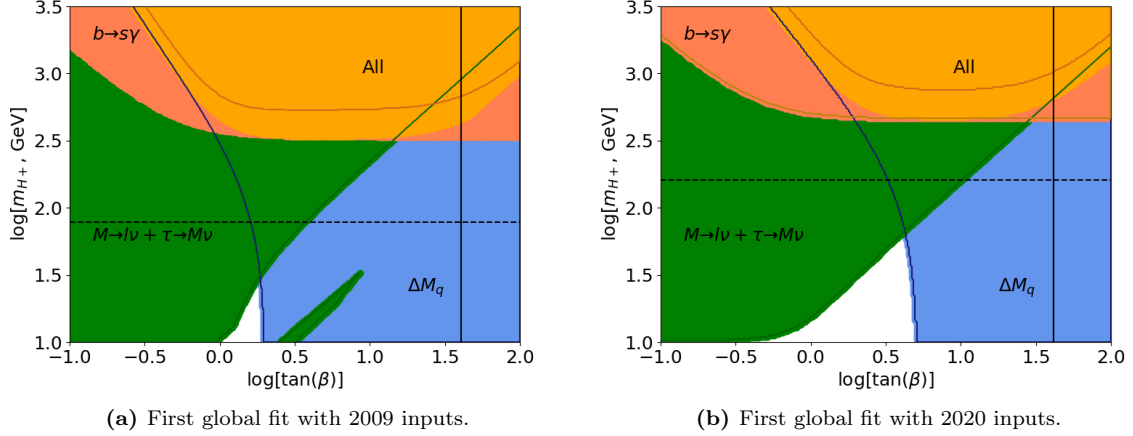


Figure 8: First global fit of constraints on m_{H^+} and $\tan\beta$ from observables considered in [24]. Each region shows what is not excluded for the relevant observables to 95% CL as discussed in the text, then the line within the orange region for all observables marks out the 1σ confidence area. The solid black vertical line shows $\tan\beta = m_t/m_b$, as for $\tan\beta$ much greater than this, the formulae for B mixing are invalid. The dashed horizontal line marks the limit from direct searches, at $m_{H^+} > 160$ GeV [29].

2.5 New Observables

Having found agreement with the fit in [24], and updating this with new inputs, we move on to new observables not yet considered. There are some observables discussed in previous works that they did not include in their fit that we discuss here, as well as some that have had improved work in experiment and theory over the last 10 years.

2.5.1 $B^+ \rightarrow \mu^+ \nu$

The heavily CKM- and helicity-suppressed leptonic decay was recently measured by the Belle collaboration [30], and can be added to the fit using the theory for leptonic decays in Section 2.1 for the first time to either reinforce the structure of the leptonic decay region in Figure 7 or to show new sensitivity. This decay is now included in the leptonic fit in Figure 7, and does not constrain the model any more than the other leptonic decays.

2.5.2 $B_{d,s} \rightarrow \mu^+ \mu^-$

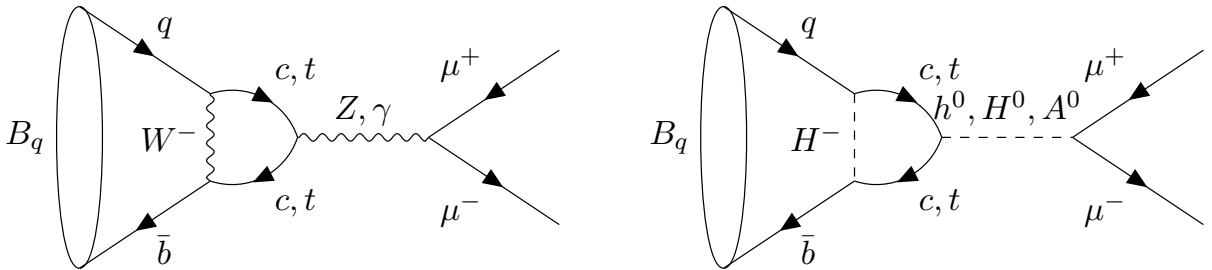


Figure 9: Examples of penguin contributions to $B_q \rightarrow \mu^+ \mu^-$ operators.

These decays can be particularly sensitive to scalar operator effects in new physics, and as such, are excellent probes for the 2HDM and the additional effects this could have.

In the 2HDM, this process is given by (for $q = d, s$)

$$\mathcal{Br}[B_q \rightarrow \mu^+ \mu^-] = \frac{G_F^4 M_W^4 s_W^4}{32\pi^5} |V_{tb}^* V_{tq}|^2 f(r^2, r^2) M_{B_q} f_{B_q}^2 (4m_\mu^2) \tau_{B_q} \times \left\{ \left| \frac{M_{B_q}^2 (C_P^* - C_P'^*)}{(m_q + m_b)(2m_\mu)} - (C_{10}^* - C_{10}'^*) \right|^2 + \left| \frac{M_{B_q}^2 (C_S^* - C_S'^*)}{(m_q + m_b)(2m_\mu)} \right|^2 [1 - 4r^2] \right\}, \quad (2.17)$$

where we follow [35] for the expressions of the relevant Wilson coefficients and the definitions of $f(x, y)$ and r , and $s_W = \sin \theta_W$ is the weak mixing angle. Previous works (see [36]) have focused on studying these processes in the large $\tan \beta$ limit ($\tan \beta \gg \sqrt{\frac{m_t}{m_b}}$) where the Yukawa coupling to b quarks is large and there can large effects on B mesons. Working in the large $\tan \beta$ limit is also useful as it reduces the number of 2HDM parameters that this process will depend on. However, in this work, we choose to work with the general expressions, as given by [35], to work with our fit across the whole parameter space we study. Using these general expressions, however, introduces new variables, primarily in the expressions for the trilinear Higgs couplings which we take from [37] and write in Eqs. B.20 and B.21. These new variables are: the masses of the neutral h^0, H^0 ; the mixing angle α ; and the 2HDM potential parameter $M = \frac{m_{12}^2}{\sin \beta \cos \beta}$ (see Eq. 1.35). These new parameters can all be varied along with m_{H^+} and $\tan \beta$ in a higher-dimensional fit, although it is simpler to fix some of these at set values.

When working in the 2HDM, it is usually assumed that we are working in the *alignment limit*, where the lighter neutral Higgs h^0 is taken to be the observed Higgs, and the mixing angles are aligned such that $\cos(\beta - \alpha) \approx 0$. Using this limit therefore allows us to fix α and m_{h^0} , leaving two additional parameters. Scanning in $(m_{H^+}, \tan \beta)$ space, as for other observables, for fixed values of M and m_{H^0} across a range based on the work in [37] and the direct searches for H^0 in [38], we find that M bears no significance on the constraints, χ_{min}^2 , or p-values of the fit. We therefore fix $M = 750$ GeV as the median value in the range considered. The value of m_{H^0} , however, does change the scan across the range chosen. We show here the impact of different values of m_{H^0} on the allowed region of parameter space at the extremities and the middle of our range. We see that there is

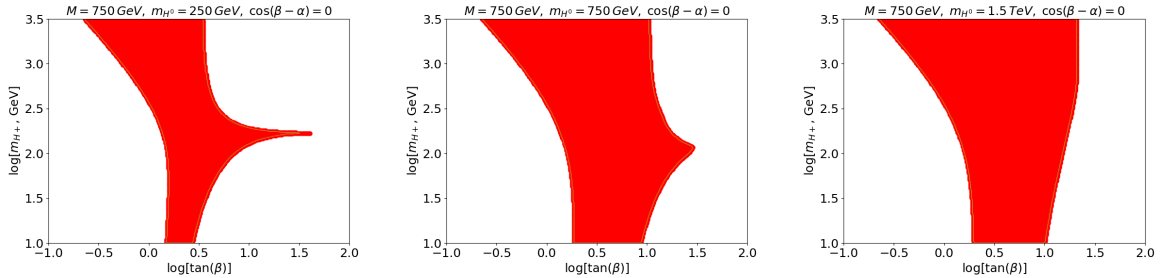


Figure 10: Constraints on $(m_{H^+}, \tan \beta)$ space from $B_{s,d} \rightarrow \mu^+ \mu^-$ decays, for $M = 750$ GeV, $\cos(\beta - \alpha) = 0$ and varying fixed values of m_{H^0} - 250 GeV (left), 750 GeV (center), 1.5 TeV (right). The red region in each plot indicates allowed parameter space after exclusion at 95% CL.

no specific constraint on m_{H^+} as we move towards ∞ , and these processes by themselves do not give a minimum value of m_{H^+} . We do however now see more significant bounds

on $\tan\beta$ than we had previously. The extent of the constraint on $\tan\beta$ depends on m_{H^0} as seen in Figure 10. When added to the global constraints, this will restrict larger $\tan\beta$ values depending on m_{H^0} . Testing across the range of values for m_{H^0} , we find that using $m_{H^0} = 1.5 \text{ TeV}$ minimises χ^2 and maximises the p-value of our fit; see Section 3 and Table 4 for details of this fit. Further analysis into this three-dimensional parameter space introduced here will be discussed in Section 2.7.

2.5.3 $\mathcal{R}(D)$ and $\mathcal{R}(D^{(*)})$

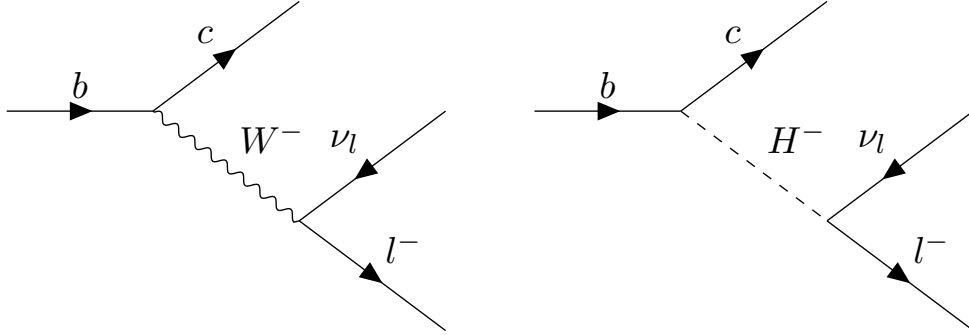


Figure 11: Tree level decay diagrams for the $b \rightarrow cl\nu$ transitions in $B \rightarrow D^{(*)}l\nu$.

These semileptonic decay ratios, defined as

$$\mathcal{R}(D^{(*)}) = \frac{\mathcal{B}r[B \rightarrow D^{(*)}\tau\nu]}{\mathcal{B}r[B \rightarrow D^{(*)}l\nu]}, \quad l = \mu, e, \quad (2.18)$$

are well-studied processes in the Standard Model, deviating from the SM predictions by 1.4σ and 2.5σ respectively [2]. Due to these deviations, these ratios seem well-suited for testing constraints on new physics models. In [24], a 2HDM parameterisation of $\mathcal{R}(D)$ was discussed and was said to align similarly with the leptonic constraints, however, they did not discuss $\mathcal{R}(D^*)$. We follow the expressions for $\mathcal{R}(D^{(*)})$ in the 2HDM found in Section III of [39] and perform a scan as before on these observables. Historically, the 2HDM

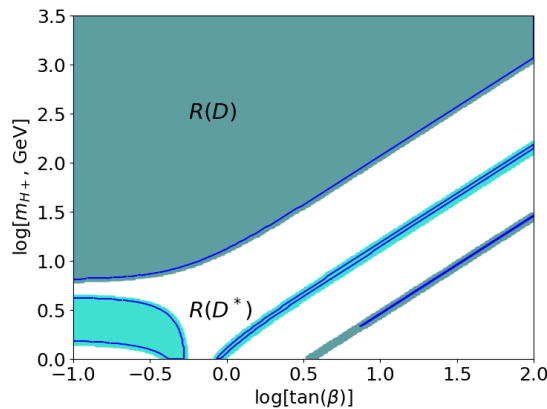


Figure 12: Constraint on $(m_{H^+}, \tan\beta)$ space from $\mathcal{R}(D)$ (blue) and $\mathcal{R}(D^*)$ (turquoise) using a 2σ scan, then χ^2 fitting as described in the text. The blue lines for each region outlines the 95% CL region.

has struggled to fit both these ratios simultaneously, and it may be a killer argument for

this model if no resolution to this can be found. So far we have implemented 2σ scans, and at this level, $\mathcal{R}(D^*)$ excludes the 2HDM, as seen in Figure 12 where $\mathcal{R}(D)$ follows a similar shape to the leptonic constraints in Figure 7 but $\mathcal{R}(D^*)$ disagrees with any region of overlap found in Figure 8b. However, exclusion at this level only means that the 2HDM performs no better than the Standard Model for this observable. We therefore move forward with two approaches to work through this discrepancy: we continue to fit all observables at the 2σ level, treating $\mathcal{R}(D^*)$ as an anomaly; and we also scan to higher σ , as $\mathcal{R}(D^*)$ may then agree with the fit to this level, leaving room for further discussion on resolving its deviation. In Figure 13, it is shown that the joint constraint from $\mathcal{R}(D)$ and $\mathcal{R}(D^*)$ aligns well with that of the leptonic decays in Figure 7 when we now scan at 3σ , but the 2HDM does fit this slightly worse than the Standard Model, as $\mathcal{R}(D^*)$ will still lead to an exclusion at 2.5σ . We test our fit with $\mathcal{R}(D^*)$ included as an anomaly at 2σ , and also include it as in Figure 13 to a 3σ scan. The statistical significance of these approaches are found in Tables 4 and 5.

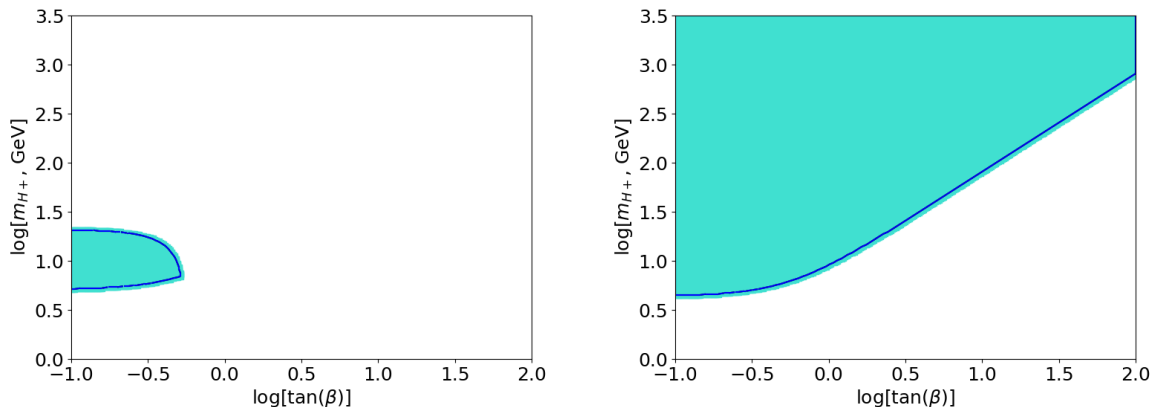


Figure 13: Constraint on $(m_{H^+}, \tan\beta)$ space from $\mathcal{R}(D)$ and $\mathcal{R}(D^*)$ from a 2.5σ scan (left) and 3σ scan (right). The turquoise region shows what is not excluded for the joint fit of these two observables from the scan, and the blue line indicates the outline of the 95% CL region.

2.6 SM4 with Two Higgs Doublet Model

As discussed in Section 1.2, a fourth generation of fermions can be proposed as a way of inducing more CP violation, but the SM4 model alone has been excluded. One proposal to still include a fourth generation is to combine this with the 2HDM. Traditionally in the 2HDM, we take the alignment limit to replicate the observed Higgs particle in the lighter neutral Higgs h of the 2HDM. This also follows from measurements of the coupling strengths of the Higgs sector, which agree with the SM predictions within 1σ [40].

There is, however, an alternate treatment to this data. LHC measurements measure the magnitudes of the couplings to closely align with the Standard Model, but they cannot determine the phase of the coupling. Defining κ_i as the ratio of the 2HDM Higgs coupling to particles ii to the SM coupling, we therefore can propose a scenario in which

$$\kappa_{W,Z} = 1, \quad \kappa_u = 1, \quad \kappa_{d,l} = -1, \quad (2.19)$$

where u denotes up-type quarks, d down-type quarks, and l the charged leptons. In this scenario, the common argument for the exclusion of the SM4 model that the gluon fusion Higgs production would be enhanced by a factor 9 over the Standard Model would no longer be valid as the new quark contributions approximately cancel each other and we recover a result close to that of the SM. This is known as the *wrong sign limit* (for a review, see e.g. [41, 42]). Within the 2HDM Type II, this limit can be written with the relationship

$$\cos(\beta - \alpha) = \sin(2\beta), \text{ or equivalently when } \tan \beta \gg 2, \cos(\beta - \alpha) = 2 \cot \beta. \quad (2.20)$$

In this work, we consider the wrong sign limit in the 2HDM only, as an indication of its validity for use in future works considering the 2HDM fit in the framework of SM4. Moving forward, in addition to working in the alignment limit as discussed previously, we consider the exact wrong sign limit from Eq. 2.20, and the use of numerical constraints on $\tan \beta$ provided from collaboration with [43]. The only observable that is dependent on the limit we choose for the Higgs couplings so far is $B_q \rightarrow \mu^+ \mu^-$, so we now look to other observables that can also compare the alignment and wrong sign limits.

2.7 The Global Fit with Oblique Parameters

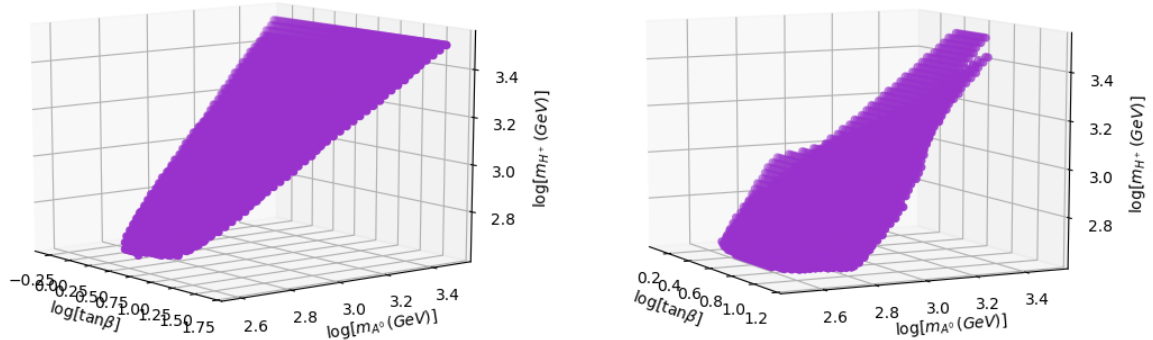


Figure 14: Constraints in $(m_{H^+}, m_{A^0}, \tan \beta)$ space from all observables, where we assume $m_{A^0} \approx m_{H^0}$, and have scanned to 2σ in the alignment limit (left) and the wrong sign limit (right). The purple region indicates what is not excluded at 95% CL.

Flavour constraints alone are not enough to give a full judgement on the 2HDM. There are other observables that can also provide indicative constraints on this model, such as the oblique parameters of the electroweak theory: S , T , U . These have not been the focus of this study, but we collaborate with [44] for their work on the oblique parameters in the 2HDM (working from the expressions given in [23, 45]), and add these to the global 2HDM fit. These observables have a different dependency on the 2HDM parameters than the flavour observables considered here, depending on $\theta = \beta - \alpha$ rather than β , α separately, as well as m_{H^0} and m_{A^0} . The value of $\beta - \alpha$ is fixed by our choice either of the alignment limit or the wrong sign limit, and we can therefore compress this dependency into that of $\tan \beta$ for these constraints. There is however still dependency on m_{H^0} and m_{A^0} to consider. We previously fixed $m_{H^0} = 1.5$ TeV, where it minimised χ^2 across the range of test values used. Due to the additional dependencies here, we perform

a test three-dimensional scan across $(m_{H^+}, m_{A^0}, \tan \beta)$ space, assuming $m_{A^0} \approx m_{H^0}$. In Figure 14, we see that there is a close linear relationship between m_{A^0} and m_{H^+} . The value of m_{H^+} is tightly constrained to be of a similar mass to m_{H^0} and m_{A^0} .³ Within the range of test values considered previously for m_{H^0} , we still find that χ^2 is minimised for $m_{H^0} = 1.5 \text{ TeV}$, so we choose to work with $m_{H^0} = m_{A^0} = 1.5 \text{ TeV}$ and test the two-dimensional global fit using these fixed parameters. Higher values than this would be even more favourable, however, we choose not to work at such high scales as discussed in Section 3.

Model:	$\cos(\beta - \alpha) = \sin(2\beta)$	$\cos(\beta - \alpha) = 0$
m_{H^+} : 95% CL	> 450	> 450
(GeV) χ^2_{min}	1900	3200
m_{A^0} : 95% CL	> 320	> 390
(GeV) χ^2_{min}	3200	3200
$\tan \beta$: 95% CL	$1.2 \rightarrow 14.3$	$0.51 \rightarrow 45.5$
χ^2_{min}	5.65	2.45
χ^2_{min}	25.4	19.2
χ^2_ν	1.82	1.37
ν	14	14
p-value	3.1%	15.8%

Table 3: Constraints and statistics for three-dimensional fit from 2σ scan in Figure 14. The fits have been done in the exact wrong-sign limit and the exact alignment limit as shown, and setting the additional 2HDM parameter $M = 750 \text{ GeV}$. For m_{H^+} , m_{A^0} and $\tan \beta$, the constraint from each model at 95% CL are shown. The information from the χ^2 fitting of each model is then shown.

3 Discussion

We now show in Figure 15 the results of our fit, for the flavour observables alone, and also including the oblique parameters from [44]. This has been done both in the alignment and wrong sign limits. As marked in the figure, it was found by [43] from perturbativity that the exact wrong sign limit is only allowed for $\tan \beta \gtrsim 6$ at the 2σ level, which significantly reduces the allowed region in our parameter space. This limit has not been included when performing the fit here, but we take note of the limitations this imposes.

It is important to have any calculations performed confirmed by an independent cross-check, and to this end, the flavour observables studied throughout have been performed as well in [46], and close agreement between results has been found, lending validity to the results we present here.

It is worth noting that, as we had in Section 2.4, the 2HDM is a decoupling theory, so as we simultaneously take $m_{H^+}, m_{H^0}, m_{A^0} \rightarrow \infty$, we will recover the Standard Model results for these processes. In the case of observables that are in agreement with the Standard Model, tending these masses to infinity will lead to a good statistical fit, as we would have in a Standard Model fit of these. Working several orders of magnitudes

³In the work of [44], it is found that there can be fine-tuned solutions away from this close confinement. However, these are for values of θ away from either the alignment or wrong sign limits we consider here.

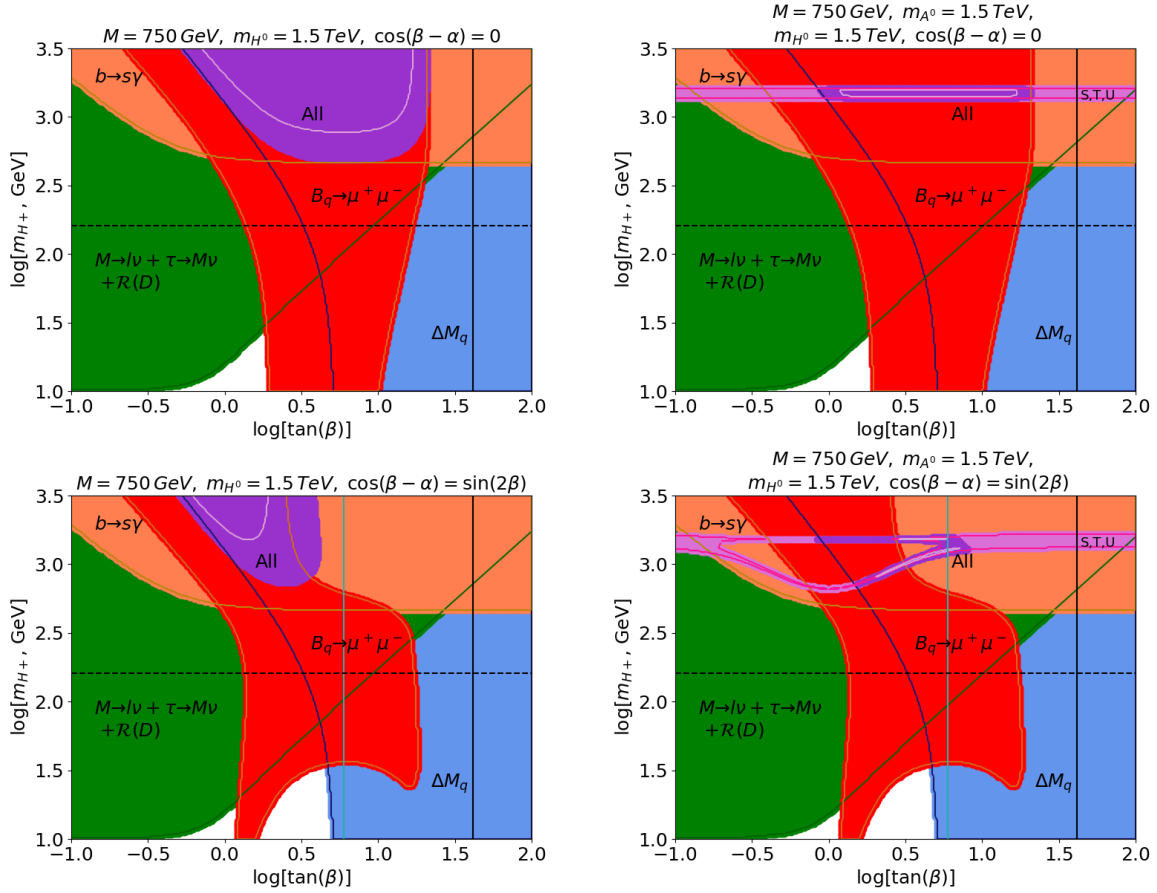


Figure 15: Constraints on $(m_{H^+}, \tan \beta)$ in the alignment limit (top) and the wrong sign limit (bottom) from 2σ scans. The constraints found in this work for flavour observables are shown (left), and then the oblique parameter constraints from [44] are included too (right). Each region shows what is not excluded for the relevant observables to 95% CL as discussed in the text - leptonic and semileptonic decays (green), B mixing (blue), $b \rightarrow s\gamma$ (orange), $B_q \rightarrow \mu^+\mu^-$ (red), and S, T, U (pink). The purple region shows our fit for all observables at 95% CL, and the white line within marks out the 1σ confidence area. The solid black vertical line shows $\tan \beta = m_t/m_b$, as for $\tan \beta$ much greater than this, the formulae for B mixing become invalid. The dashed horizontal line marks the limit for a charged Higgs from direct searches, at $m_{H^+} > 160$ GeV [29]. For this two-dimensional fit, we fix the additional 2HDM parameters as in the titles of the plots and described in the text. For the wrong sign limit, we use the exact form given in Eq. 2.20, and mark with the vertical turquoise line the lower limit of its validity, as found by [43]. The upper and lower bounds on parameters and the statistical indicators for each fit are shown in Table 4.

above the mass scales of the other particles approximates this limit to infinity, so to test a physical, and observable, Two Higgs Doublet Model Type II which is significant against the Standard Model, it is of no use looking to such large scales so we therefore remain working with more relevant mass scales as chosen for m_{H^0} and m_{A^0} . This effect is also seen in the χ^2 fitting in Tables 3, 4, and 5. The value of m_{H^+} that minimises χ^2 for flavour observables alone and fixed m_{H^0} is 3200 GeV, and similarly for m_{A^0} and m_{H^+} in the three-dimensional global fit. These values are not representative of what would actually minimise χ^2 across any value these parameters could take, but rather χ^2_{min} within the range chosen, where we do not scan higher than 3200 GeV for any mass. Were we to scan higher than this, we would expect a similar result whereby the values of m_{H^+} and m_{A^0} which minimise χ^2 would be the highest value scanned to, and so on to the decoupling

limit of this model. The wrong sign limit, however, shows a different result for m_{H^+} in our three-dimensional fit, where it minimises χ^2 at 1900 GeV. This is due to the upper and lower regions the oblique parameters have in this limit.

We show in Table 4 the numerical constraints found in our parameter space from Figure 15, and the statistical significance of the various fits. Due to the discrepancy found in $\mathcal{R}(D^*)$, different approaches were taken to explore its impact on the fit: in Table 4, the statistical indicators for including this as an anomaly at 2σ are given, and then in brackets we give the indicators for a fit disregarding $\mathcal{R}(D^*)$, such that we see the sole impact of this observable; we also show in Table 5 how the values of the constraints of our fit change for a 3σ scan as opposed to a 2σ scan, where $\mathcal{R}(D^*)$ now fits well with other constraints, as shown in Figure 13. The effect of $\mathcal{R}(D^*)$ at 2σ is clear. Including $\mathcal{R}(D^*)$

Model:	$\cos(\beta - \alpha) = \sin(2\beta)$		$\cos(\beta - \alpha) = 0$	
	Flavour	Flavour + Oblique	Flavour	Flavour + Oblique
m_{H^+} : 95% CL	> 740	$720 \rightarrow 1580$	> 490	$1380 \rightarrow 1620$
(GeV) 1σ	> 1510	$790 \rightarrow 1540$	> 770	$1410 \rightarrow 1580$
χ^2_{min}	3200	1510	3200	1440
$\tan\beta$: 95% CL	< 4.03	$0.84 \rightarrow 8.1$	< 20.8	$0.88 \rightarrow 20.8$
1σ	< 1.92	$1.1 \rightarrow 7.7$	< 16.9	$1.2 \rightarrow 16.9$
χ^2_{min}	0.98	1.9	4.1	5.2
χ^2_{min}	20.6 (11.5)	25.6 (16.6)	18.8 (9.78)	19.4 (10.3)
χ^2_ν	1.7 (1.0)	1.7 (1.2)	1.6 (0.9)	1.3 (0.7)
ν	12 (11)	15 (14)	12 (11)	15 (14)
p-value	5.7% (40%)	4.2% (28%)	9.3% (55%)	20% (74%)

Table 4: Constraints and statistics for global fits following 2σ scans. ‘Flavour’ denotes all of the flavour observables discussed throughout, including $\mathcal{R}(D^*)$ as an anomaly; ‘Oblique’ denotes adding the three oblique parameters from [44]. The fits have been done in the exact wrong-sign limit and the exact alignment limit as shown, and setting the additional 2HDM parameters as $M = 750$ GeV and $m_{H^0} = m_{A^0} = 1.5$ TeV. For m_{H^+} and $\tan\beta$, the constraints from each model at 95% CL and 1σ and their χ^2_{min} values are shown respectively. The information from the χ^2 fitting of each model is then shown, first for the inclusion of $\mathcal{R}(D^*)$ in this fit, and then in brackets we show the fit were we to exclude $\mathcal{R}(D^*)$. The 2HDM potential parameter M does not impact the fit as it varies, although through the oblique parameters, m_{H^0} and m_{A^0} will cause our results to vary as these require all new Higgs masses to be approximately equal, thus confining the space tightly near whatever values are chosen for these masses. The constraints, therefore, which include the oblique parameters are test constraints for fixed $m_{H^0} = m_{A^0}$ as above, and not indicative of global constraints. The flavour alone constraints, however, do give a minimum constraint of m_{H^+} with no extra dependency.

almost doubles χ^2_{min} in most of the cases shown, and heavily reduces the p-values for these fits, taking them from where we might still consider the 2HDM a possible physical theory, to where we now consider exclusion of this model (under the conditions imposed here). We do not propose any further solution to the problem of $\mathcal{R}(D^*)$ here, though we recognise one must be found if the Two Higgs Doublet Model Type II could still be considered.

We show the details of the 3σ fit in Table 5. At this level, all scenarios we consider fit much better than at 2σ , and we cannot consider exclusion at the 3σ error significance. However, we do see in χ^2_ν and the p-values that although the errors do not yet fully dominate, they are significant enough that we begin to lose the resolution in our results at this level. We continue to consider the fit at 2σ , where we can find statistical insight into our results.

Due to the additional dependencies from the oblique parameters, we cannot conclude many limitations in our $(m_{H^+}, \tan\beta)$ parameter space, apart from that H^+ must have a similar mass to H^0 and A^0 . The most definitive constraints on m_{H^+} and $\tan\beta$ come from the $b \rightarrow s\gamma$ radiative decay and $B_q \rightarrow \mu^+\mu^-$ respectively. The flavour constraints in Table 4 show the minimum value for m_{H^+} that is primarily constrained from $b \rightarrow s\gamma$, and also show the maximum $\tan\beta$ as constrained from $B_q \rightarrow \mu^+\mu^-$. This $\tan\beta$ constraint is, however, dependent on m_{H^0} , and is therefore not conclusive due to the lack of constraint on this parameter. The maximum allowed value for $\tan\beta$ is seen to increase with larger m_{H^0} in the alignment limit, as shown in Figure 14, and so, this is only indicative of the limitations for $\tan\beta$ for the more finite masses we consider.

Overall, the statistical indicators of our fit including all observables at the 2σ level show that the likelihood of the 2HDM being physical is very low. First, when considering the 2HDM in the wrong sign limit, both for flavour observables alone, and for flavour with the oblique parameters, the p-values show exclusion to $\approx 95\%$ CL. This is also the case in the three-dimensional fit. The likelihood therefore of this model being correct is slim. This model would likely perform even worse statistically were we to include the $\tan\beta \gtrsim 6$ limit from [43] in the fit, as the current χ^2_{min} value for the ranges of $\tan\beta$ given in Tables 3 and 4 is found at $\tan\beta < 6$ in all cases, and as such, we would expect an increased value for χ^2_{min} from imposing this limit and a further decrease in the p-value. In the case of the flavour observables alone in the wrong sign limit, $\tan\beta$ is restricted from taking values greater than 14.3 at 95% CL, and although including the constraint from [43] may change the fit, it is unlikely to increase the maximum $\tan\beta$ significantly for these observables, in which case, the wrong sign limit is fully excluded from the comparison of flavour observable constraints and the perturbativity constraints from [43]. There would still be some allowed space when including the oblique parameters in the fit for the wrong sign limit, however, this will be a very narrow region, and the confidence in this will be much smaller. As can be seen in Figure 15, the behaviour of the oblique parameters causes two separate allowed regions for lower $\tan\beta$, although they do combine above the $\tan\beta \gtrsim 6$ threshold we consider. This strange behaviour can be neglected in this limit, but it could be possible that it does have a more significant impact under further study.

The dependency on m_{H^0} in the wrong sign limit differs from the alignment limit, with the constraint from $B_q \rightarrow \mu^+\mu^-$ taking a different shape, that may actually favour lower values of m_{H^0} as this would result in an increase in the allowed range for $\tan\beta \gtrsim 6$. While we are still limited to a minimum value for m_{H^+} (and consequently m_{H^0} for $m_{H^0} \approx m_{H^+}$) from $b \rightarrow s\gamma$, approaching this minimum value could increase the prospects of realising the wrong sign limit. We see this in the three-dimensional fit in Figure 14 and Table 3 where there is a larger region allowed for $\tan\beta > 6$, particularly for lower values of m_{H^+} and m_{A^0} . These lower values are also not as constrained in the wrong sign limit, as we

see χ^2 can be minimised without tending towards infinity for m_{H^+} as much as in the alignment limit.

Working in the alignment limit, the fit performs better statistically than in the wrong sign limit, however, it does not overall perform well, as it is excluded at 90% CL for the flavour constraints, and the joint flavour and oblique constraints are excluded at 80% CL. In the three-dimensional fit for all observables, it is excluded at 85% CL. As discussed above, $\mathcal{R}(D^*)$ proves to be the undoing of this model. When excluding it from the fit, we find agreeable results for both flavour alone and including the oblique parameters (though we must be careful as for the latter, the errors may be too large). However, when including $\mathcal{R}(D^*)$, as is important to do for the global fit, these results significantly decrease and we must begin to question this model. The allowed parameter space for these conditions is rather slim, as seen in Figure 15, however, this is due to the fixing of $m_{H^0} \approx m_{A^0}$, whereas in Figure 14, we can see this space tend to infinity when allowing these masses to vary too. The main constraints we are left with, therefore, are still that shown for the flavour alone considerations in Table 4, primarily from $b \rightarrow s\gamma$, while also considering the direct searches for these particles, as in [29, 38].

An interesting contrast between the two limits of the 2HDM discussed is that in the wrong sign limit, combining the flavour and oblique constraints reduces the confidence of the model in comparison to the flavour constraints alone, whereas in the alignment limit, including the oblique constraints actually improves the confidence of the model. A more focused study on the oblique parameters, such as that of [44], would likely yield more information from this contrast, where the wrong sign limit more poorly fits the oblique parameters than it does the flavour observables. The flavour observables do fit worse in the wrong sign limit than in the alignment limit, although the contrast is not as severe as when including the oblique parameters. The oblique parameters hold a lot more importance in our choice of $\beta - \alpha$ than the flavour observables, and a more extensive look into their variation due to $\beta - \alpha$ would prove interesting (we again turn to [44], where this has been more in focus in their study). It could perhaps be the case that $\beta - \alpha$ does not fall into either of the cases discussed here; even though they seem the most apparent to consider, nature may have found a better choice if this model is correct. In certain cases away from the $\beta - \alpha$ constraints considered here, it is also possible to allow the masses of H^0 , A^0 , and H^+ to be less tightly confined near a single value. This could cause interesting changes in the 2HDM global fit in future works.

3.1 Future Prospects

While we have attempted to be thorough in our analysis of the 2HDM and its fit to flavour observables (and oblique parameters), and we have found certain definitive statements on the validity of this model, we cannot say these are conclusive yet. In fact, this study has suggested that there is more work to be done for a global fit of the 2HDM, to combine with our findings here. Due to time limitations on this study, we have not included everything in our work here, but we recognise that there are clear additions that could bear importance in future work.

First, our list of flavour observables used here is not extensive by any means, and there are still many processes we could consider and add to the fit. Most noticeably,

Model:	$\cos(\beta - \alpha) = \sin(2\beta)$		$\cos(\beta - \alpha) = 0$	
	Flavour	Flavour + Oblique	Flavour	Flavour + Oblique
m_{H^+} (GeV): 95% CL	> 310	$690 \rightarrow 1690$	> 300	$1380 \rightarrow 1620$
1σ	> 850	$740 \rightarrow 1620$	> 520	$1380 \rightarrow 1620$
χ^2_{min}	3200	1510	3200	1440
$\tan \beta$: 95% CL	no constraint	$0.7 \rightarrow 55$	< 25	$0.7 \rightarrow 25$
1σ	< 3.2	$0.9 \rightarrow 28$	< 20	$0.9 \rightarrow 20$
χ^2_{min}	0.98	1.9	4.1	5.2
χ^2_{min}	9.16	11.4	8.36	8.62
χ^2_ν	0.76	0.76	0.70	0.57
ν	12	15	12	15
p-value	68.9%	72.4%	75.6%	89.7%

Table 5: Constraints and statistics for global fits following 3σ scans. ‘Flavour’ denotes all of the flavour observables discussed throughout, including $R(D^*)$ which fits to this level; ‘Oblique’ denotes adding the three oblique parameters from [44]. The fits have been done in the exact wrong-sign limit and the exact alignment limit as shown, and setting the additional 2HDM parameters as $M = 750$ GeV and $m_{H^0} = m_{A^0} = 1.5$ TeV. For m_{H^+} and $\tan \beta$, the constraints from each model at 95% CL and 1σ and their χ^2_{min} values are shown respectively. The information from the χ^2 fitting of each model is then shown. The 2HDM potential parameter M does not impact the fit as it varies, although through the oblique parameters, m_{H^0} and m_{A^0} cause our results to vary as these require all new Higgs masses to be approximately equal, thus confining the space tightly near whatever values are chosen for these masses.

the ratios $\mathcal{R}(K^{(*)})$ present interesting opportunities to further test our constraints on the 2HDM. Recent work on expressions for these observables in the 2HDM can be found, for example, in [35].

The wrong sign limit in the 2HDM alone was considered here as an indicator towards the possibility of SM4×2HDM as a resolution to the long-standing issues of the standard SM4 extension. We here found that the wrong sign limit is effectively excluded for the 2HDM alone, which does not bode well for a full consideration of SM4×2HDM. However, we cannot guarantee that the inclusion of the SM4 contributions to the observables here would not change the fit significantly enough such that this model is not entirely excluded. A full extension of this study into SM4×2HDM in the wrong sign limit would be the clear next step from our findings here.

4 Conclusions

We have tested the Two Higgs Doublet Model Type II using flavour observables, where we have looked for constraints on m_{H^+} and $\tan \beta$. The constraints found from flavour observables are outlined in Table 4 in both the alignment and wrong sign limits, using 2σ scans. We have also collaborated with [44] to include the oblique parameters S, T, U into our fit, where the most definitive constraint found with this is that $m_{H^+} \approx m_{H^0} \approx m_{A^0}$. Details of this fit are found in Tables 3 and 4. We have found that we can exclude this model at 2σ error significance to 95% CL in the wrong sign limit, and 85% CL in the

alignment - this was found both in a two-dimensional fit with fixed $m_{H^0} = m_{A^0}$, and a three-dimensional fit varying m_{H^0} . The model cannot be excluded with large confidence at 3σ error significance. The most significant effect towards the poor fitting of this model is the semileptonic ratio $\mathcal{R}(D^*)$, which disagrees with our 2HDM fit to 3σ . Without this ratio, this model cannot be excluded to a high CL, but including it significantly increases the confidence of exclusion. No resolution to this problem is found here, though we hope that future works may either find one, or confirm its use to exclude the 2HDM.

Acknowledgments

Thanks is given to Prof. Alexander Lenz for his sage advice and guidance throughout the year, and also to Aleksey Rusov for his assistance. I also thank Oliver Atkinson, James Wynne, and Tom Eaton for their collaborating efforts and many fruitful discussions.

References

- [1] S. Glashow, *Partial Symmetries of Weak Interactions*, Nucl. Phys. **22** (1961) 679; S. Weinberg, *A Model Of Leptons*, Phys. Rev. Lett. **19** (1967) 1294; A. Salam, *Weak and Electromagnetic Interactions*, Conf. Proc. C **680519** (1968) 367.
- [2] M. Tanabashi et al [Particle Data Group], Phys. Rev. D98 030001 (2018) and 2019 update.
- [3] D. Gross and F. Wilczek, *Ultraviolet Behavior of Non-Abelian Gauge Theories*, Phys. Rev. Lett. **30** (1973) 1343-1346.
- [4] M. Schwartz, *Quantum Field Theory and the Standard Model* (Cambridge University Press, 2018).
- [5] T. Lee and C. Yang, *Question of Parity Conservation in Weak Interactions*, Phys. Rev. **104** (1956) 254-258.
- [6] C. Wu et al, *Experimental Test of Parity Conservation in β Decay*, Phys. Rev. **105** (1957), 1413-1414.
- [7] P. W. Higgs, *Broken Symmetries and the Masses of Gauge Bosons*, Phys. Rev. Lett. **13** (1964) 508-509; F. Englert and R. Brout, *Broken Symmetry and the Mass of Gauge Vector Mesons*, Phys. Rev. Lett. **13** (1964) 321-323; G. Guralnik, C. Hagen and T. Kibble, *Global Conservation Laws and Massless Particles*, Phys. Rev. Lett. **13** (1964) 585-587.
- [8] M. Peskin and D. Schroeder, *An Introduction to Quantum Field Theory* (CRC Press, 2019).
- [9] M. Kobayashi and T. Maskawa, *CP Violation in the Renormalizable Theory of Weak Interaction*, Prog. Theor. Phys. **49** (1973) 652-657.
- [10] L. Wolfenstein, *Parametrization of the Kobayashi-Maskawa Matrix*, Phys. Rev. Lett. **51** (1983).
- [11] N. Cabibbo, *Unitary Symmetry and Leptonic Decays*, Phys. Rev. Lett. **10** (1963) 531-533.
- [12] CKMfitter Group (J. Charles et al.), Eur. Phys. J. C41, 1-131 (2005) [hep-ph/0406184], updated results and plots available at: <http://ckmfitter.in2p3.fr>.

- [13] A. Sakharov, *Violation of CP Invariance, C asymmetry, and Baryon Asymmetry of the Universe*, Pisma Zh. Eksp. Teor. Fiz. **5** (1967) 32 [JETP Lett. **5** (1967) 24] [Sov. Phys. Usp. **34** (1991) 392] [Usp. Fiz. Nauk **161** (1991) 61].
- [14] F. R. Klinkhamer and N. Manton, *A Saddle Point in the Weinberg-Salam Theory*, Phys. Rev. D **30** (1984) 2212.
- [15] K. Kajantie, M. Laine, K. Rummukainen, and M. Shaposhnikov, *Is There a Hot Electroweak Phase Transition at $m_H \gtrsim m_W$?*, Phys. Rev. Lett. **77** (1996) 2887-2890, [[arXiv:9605288 \[hep-ph\]](#)].
- [16] J. Christenson et al, *Evidence for the 2π Decay of the K_2^0 Meson*, Phys. Rev. Lett. **13** (1964), 138-140.
- [17] M. Artuso, G. Borissov, and A. Lenz, *CP Violation in the B_s^0 system*, Rev. Mod. Phys. **88** (2016) no.4 045002, [[arXiv:1511.09466 \[hep-ph\]](#)].
- [18] R. Aaij et al, *Observation of CP Violation in Charm Decays*, Phys. Rev. Lett. **122** (2019) no.21 211803, [[arXiv:1903.08726 \[hep-ex\]](#)].
- [19] T.G. Rizzo, *Z' Phenomenology and the LHC*, [[arXiv:0610104 \[hep-ph\]](#)].
- [20] A. Lenz, *Constraints on a Fourth Generation of Fermions from Higgs Boson Searches*, Adv. High Energy Phys. **2013** (2013) 910275.
- [21] S. Bar-Shalom, M. Geller, S. Nandi, and A. Soni, *Two Higgs doublets, a 4th generation and a 125 GeV Higgs: a review*, Adv. High Energy Phys. **2013** (2013) 672972, [[arXiv:1208.3195 \[hep-ph\]](#)].
- [22] G.C. Branco et al, *Theory and phenomenology of two-Higgs-doublet models*, Phys. Rept. **516** (2012) 1-102, [[arXiv:1106.0034 \[hep-ph\]](#)].
- [23] J. Gunion, H. Haber, G. Kane and S. Dawson, *The Higgs Hunter's Guide* (CRC Press, 2018).
- [24] O. Deschamps et al [CKMfitter], *The Two Higgs Doublet Model of Type II facing flavour physics data*, Phys. Rev. D **82** (2010) 073012, [[arXiv:0907.5135 \[hep-ph\]](#)].
- [25] J. Urban, F. Krauss, U. Jentschura and G. Soff, *Next-to-Leading Order QCD corrections for the $B^0\bar{B}^0$ -mixing with an extended Higgs sector*, Nucl. Phys. B **523** (1998) 40-58, [[arXiv:9710245 \[hep-ph\]](#)].
- [26] L. Di Luzio, M. Kirk, A. Lenz and T. Rauh, *ΔM_s theory precision confronts flavour anomalies*, JHEP **12** (2019) 009, [[arXiv:1909.11087 \[hep-ph\]](#)].
- [27] M. Misiak and M. Steinhauser, *NNLO QCD Corrections to the $\bar{B} \rightarrow X_s \gamma$ Matrix Elements Using Interpolation in m_c* , Nucl. Phys. B **764** (2007) 62-82, [[arXiv:0609241 \[hep-ph\]](#)].
- [28] G. Degrandi, P. Gambino, and P. Slavich, *SusyBSG: a fortran code for BR[$B \rightarrow X_s \gamma$] in the MSSM with Minimal Flavor Violation*, Comput. Phys. Commun. **179** (2008) 759-771, [[arXiv:0712.3265 \[hep-ph\]](#)].
- [29] M. Aaboud et al [ATLAS], *Search for charged Higgs bosons decaying via $H^\pm \rightarrow \tau^\pm \nu_\tau$ in the τ +jets and τ +lepton final states with 36 fb^{-1} of pp collision data recorded at $\sqrt{s} = 14\text{ TeV}$ with the ATLAS experiment*, JHEP **09** (2018) 139, [[arXiv:1807.07915 \[hep-ex\]](#)].

- [30] M. T. Prim et al [Belle Collaboration], *Search for $B^+ \rightarrow \mu^+ \nu_\mu$ and $B^+ \rightarrow \mu^+ N$ with inclusive tagging*, Phys. Rev. D **101** (2020) no.3 032007, [[arXiv:1911.03186 \[hep-ex\]](#)].
- [31] Y. Amhis et al [HFLAV], *Averages of b -hadron, c -hadron, and τ -lepton properties as of 2018*, [[arXiv:1909.12524 \[hep-ex\]](#)].
- [32] A. Sibidanov et al [Belle], *Study of Exclusive $B \rightarrow X_u l \nu$ Decays and Extraction of $|V_{ub}|$ using Full Reconstruction Tagging at the Belle Experiment*, Phys. Rev. D **88** (2013) no.3 032005, [[arXiv:1306.2781 \[hep-ex\]](#)].
- [33] S. Aoki et al [FLAG], *FLAG Review 2019*, Eur. Phys. J. C **80** (2020) no.2 113, [[arXiv:1902.08191 \[hep-lat\]](#)].
- [34] A. Lenz, private correspondence.
- [35] A. Crivellin, D. Müller, and C. Wiegand, *$b \rightarrow sl^+ l^-$ transitions in two-Higgs-doublet models*, JHEP **06** (2019) 119, [[arXiv:1903.10440 \[hep-ph\]](#)].
- [36] H. E. Logan and U. Nierste, *$B_{s,d} \rightarrow l^+ l^-$ in a two Higgs doublet model*, Nucl. Phys. B **586** (2000) 39-55, [[arXiv:0004139 \[hep-ph\]](#)].
- [37] P. Arnan, D. Bečirević, F. Mescia, and O. Sumensari, *Two Higgs doublet models and $b \rightarrow s$ exclusive decays*, Eur. Phys. J. C **77** (2017) no.11 796, [[arXiv:1703.03426 \[hep-ph\]](#)].
- [38] A. M. Sirunyan et al [CMS], *Search for MSSM Higgs bosons decaying to $\mu^+ \mu^-$ in proton-proton collisions at $s = 13$ TeV*, Phys. Lett. B **798** (2019) 134992, [[arXiv:1907.03152 \[hep-ex\]](#)].
- [39] J. Lee, *$B \rightarrow D^{(*)} \tau \nu_\tau$ in the 2HDM with an anomalous τ coupling*, Phys. Rev. D **96** (2017) no.5 055005, [[arXiv:1705.02465 \[hep-ph\]](#)].
- [40] A. M. Sirunyan et al [CMS], *Combined measurements of Higgs boson couplings in proton-proton collisions at $\sqrt{s} = 13$ TeV*, Eur. Phys. J. C **79**(2019) no.5 421, [[arXiv:1809.10733 \[hep-ex\]](#)].
- [41] D. Das, A. Kundu and I. Saha, *Higgs data does not rule out a sequential fourth generation with an extended scalar sector*, Phys. Rev. D **97** (2018) no.1 011701, [[arXiv:1707.03000 \[hep-ph\]](#)].
- [42] M. Raju, J. P. Saha, D. Das and A. Kundu, *Double Higgs production as an exclusive probe for a sequential fourth generation with wrong-sign Yukawa couplings*, Phys. Rev. D **101** (2020) no.5 055036, [[arXiv:2001.05280 \[hep-ph\]](#)].
- [43] O. Atkinson, private correspondence.
- [44] J. Wynne, private correspondence.
- [45] W. Grimus, L. Lavoura, O. Og Reid and P. Osland, *The Oblique parameters in multi-Higgs models*, Nucl. Phys. B **801** (2008) 81-96, [[arXiv:0802.4353 \[hep-ph\]](#)].
- [46] T. Eaton, private correspondence.

A Plots of 3σ scans

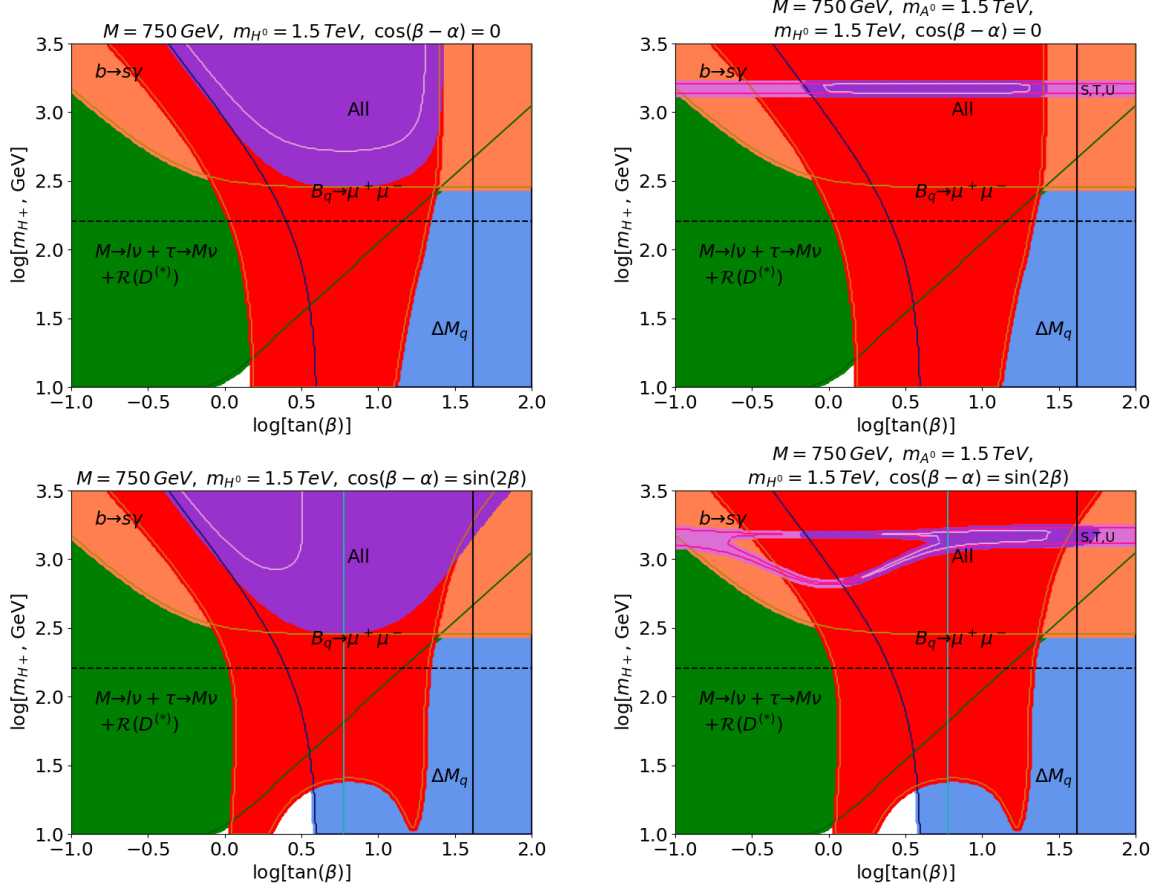


Figure 16: Constraints on $(m_{H^+}, \tan \beta)$ in the alignment limit (top) and the wrong sign limit (bottom) from 3σ scans. The constraints found in this work for flavour observables are shown (left), and then the oblique parameter constraints from [44] are included too (right). Each region shows what is not excluded for the relevant observables to 95% CL as discussed in the text - leptonic and semileptonic decays (green), B mixing (blue), $b \rightarrow s\gamma$ (orange), $B_q \rightarrow \mu^+ \mu^-$ (red), and S, T, U (pink). The purple region shows our fit for all observables at 95% CL, and the white line within marks out the 1σ confidence area. The solid black vertical line shows $\tan \beta = m_t/m_b$, as for $\tan \beta$ much greater than this, the formulae for B mixing become invalid. The dashed horizontal line marks the limit for a charged Higgs from direct searches, at $m_{H^+} > 160$ GeV [29]. For this two-dimensional fit, we fix the additional 2HDM parameters as in the titles of the plots and described in the text. For the wrong sign limit, we use the exact form given in Eq. 2.20, and mark with the vertical turquoise line the lower limit of its validity, as found by [43]. The upper and lower bounds on parameters and the statistical indicators for each fit are shown in Table 5.

B Relevant Feynman Rules in the SM and 2HDM

We show here some of the relevant Feynman rules for the couplings in the Standard Model and in the 2HDM. We follow [8] for the SM expressions, and [23] and [37] for the 2HDM expressions.

Propagators:

$$\text{---}\overset{f}{\rightarrow}\text{---} = \frac{i(\not{p} + m)}{p^2 - m^2 + i\epsilon} \quad (\text{B.1})$$

$$\text{~~~~~}\overset{\gamma}{\text{~~~~~}} = \frac{-ig^{\mu\nu}}{p^2 + i\epsilon} \quad (\text{B.2})$$

$$\text{~~~~~}\overset{G}{\text{~~~~~}} = \frac{-ig^{\mu\nu}}{p^2 + i\epsilon} \quad (\text{B.3})$$

$$\text{~~~~~}\overset{X}{\text{~~~~~}} = \frac{-ig^{\mu\nu}}{p^2 - m_X^2 + i\epsilon} \quad (\text{B.4})$$

$$\text{-----}\overset{\varphi}{\text{-----}} = \frac{i}{p^2 - m^2 + i\epsilon} \quad (\text{B.5})$$

Electroweak and Strong Vertices:

$$\begin{array}{c} \text{---}\overset{f}{\rightarrow} \\ \text{---}\overset{\bar{f}}{\rightarrow} \end{array} \text{---}\overset{\gamma}{\text{~~~~~}} = -ieQ\gamma^\mu \quad (\text{B.6})$$

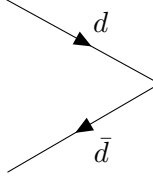
$$\begin{array}{c} \text{---}\overset{l^-}{\rightarrow} \\ \text{---}\overset{\bar{\nu}_l}{\rightarrow} \end{array} \text{---}\overset{W^-}{\text{~~~~~}} = \frac{-ie}{\sqrt{2}\sin\theta_w}\gamma^\mu P_L \quad (\text{B.7})$$

$$\begin{array}{c} \text{---}\overset{d^j}{\rightarrow} \\ \text{---}\overset{\bar{u}^i}{\rightarrow} \end{array} \text{---}\overset{W^-}{\text{~~~~~}} = \frac{-ie}{\sqrt{2}\sin\theta_w}\gamma^\mu P_L V_{ij}^* \quad (\text{B.8})$$

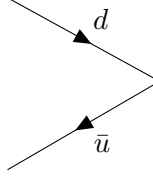
$$\begin{array}{c} \text{---}\overset{q_\beta^j}{\rightarrow} \\ \text{---}\overset{\bar{q}_\alpha^i}{\rightarrow} \end{array} \text{~~~~~} = ig\gamma_\mu T_{ij}^\alpha \delta_{\alpha\beta} \quad (\text{B.9})$$

2HDM Higgs Vertices:

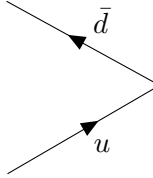
$$\begin{array}{c} \text{---}\overset{u}{\rightarrow} \\ \text{---}\overset{\bar{u}}{\rightarrow} \end{array} \text{-----}\overset{h^0}{\text{-----}} = -\frac{im_u \cos\alpha}{v \sin\beta} \quad (\text{B.10})$$



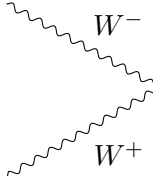
$$h^0 = \frac{im_d \sin \alpha}{v \cos \beta} \quad (\text{B.11})$$



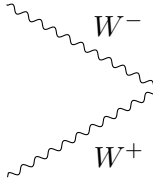
$$H^+ = \frac{ig}{2\sqrt{2}m_W} [(m_d \tan \beta + m_u \cot \beta) - (m_d \tan \beta - m_u \cot \beta)\gamma_5] \quad (\text{B.12})$$



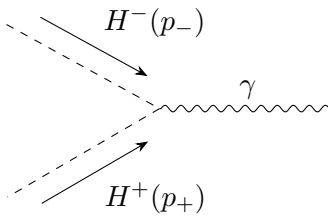
$$H^- = \frac{ig}{2\sqrt{2}m_W} [(m_d \tan \beta + m_u \cot \beta) + (m_d \tan \beta - m_u \cot \beta)\gamma_5] \quad (\text{B.13})$$



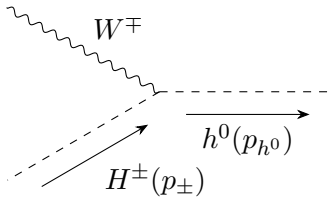
$$h^0 = igm_W \sin(\beta - \alpha)g^{\mu\nu} \quad (\text{B.14})$$



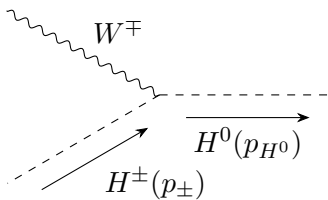
$$H^0 = igm_W \cos(\beta - \alpha)g^{\mu\nu} \quad (\text{B.15})$$



$$\gamma = ie(p_- - p_+)^\mu \quad (\text{B.16})$$



$$h^0(p_{h^0}) = \pm \frac{ig}{2} \cos(\beta - \alpha)(p_{H^\pm} + p_{h^0})^\mu \quad (\text{B.17})$$



$$H^0(p_{H^0}) = \mp \frac{ig}{2} \cos(\beta - \alpha)(p_{H^\pm} + p_{H^0})^\mu \quad (\text{B.18})$$

$$= \frac{g}{2}(p_{H^\pm} + p_{A^0})^\mu \quad (\text{B.19})$$

$$= \frac{-i}{2v \sin(2\beta)} \left\{ m_{h^0}^2 [3 \cos(\alpha + \beta) + \cos(\alpha - 3\beta)] + 4 \sin(2\beta) \sin(\beta - \alpha) m_{H^\pm}^2 - 4M^2 \cos(\alpha + \beta) \right\} \quad (\text{B.20})$$

$$= \frac{-i}{2v \sin(2\beta)} \left\{ m_{H^0}^2 [3 \sin(\alpha + \beta) + \sin(\alpha - 3\beta)] + 4 \sin(2\beta) \sin(\beta - \alpha) m_{H^\pm}^2 - 4M^2 \sin(\alpha + \beta) \right\} \quad (\text{B.21})$$

For the labels of the Feynman diagrams, we use the following conventions:

Label	Meaning
f	any fermion
γ	photon
G	gluons
X	any massive boson
φ	any scalar boson
l	charged lepton
u	any up-type quark
d	any down-type quark
i, j	quark flavour index
α, β	quark colour index

Table 6: Conventions for labels of Feynman diagrams.

Note that in Eqs. [B.10](#) and [B.11](#), we will recover the SM result for this vertex in the decoupling solution of the 2HDM, i.e. $v_2 \rightarrow 0, \beta \rightarrow 0, \alpha \rightarrow -\frac{\pi}{2}$.